MULTIDECADAL EVOLUTION IN VELOCITY AND ICE THICKNESS OF ILLAULITTUUQ (CORONATION) AND MAATTATUJANA (MAKTAK) GLACIERS, BAFFIN ISLAND NUNAVUT

DOMYNIK HUOT

Thesis submitted to the University of Ottawa
in partial Fulfillment of the requirements for the
Master of Science degree in Geography

Department of Geography, Environment and Geomatics
Faculty of Arts
University of Ottawa

Abstract

Marine-terminating glaciers often respond dynamically to ocean forcing, but Illaulittuuq Glacier, a primary calving outlet of Penny Ice Cap, is shifting towards behaviour more like its neighbouring land-terminating counterpart, Maattatujana Glacier. From 1958 to 2024, both glaciers retreated, thinned, and decelerated in similar fashion despite their contrasting terminus types. Illaulittuuq's retreat accelerated after the mid-1990s, while Maattatujana's response occurred later, yet both now lose mass at comparable rates and show similar velocity profiles with highest speeds in the upper ablation zone, decreasing rapidly toward their termini. Most revealing is Illaulittuuq's shifting mass budget: dynamic discharge accounted for nearly half of total mass losses in 2000-04 but <3% by 2020-24, even as total mass loss intensified. Sustained thinning was the dominant driver of velocity change at both glaciers, reducing basal sliding, particularly during spring and summer, and shifting flow toward internal deformation as ice thins and driving stress declines.

Acknowledgements

I am grateful to the community of Qikiqtarjuaq, notably Billy and Daisy Arnaquq, for welcoming me on their traditional land and facilitating fieldwork in the region. Their knowledge of the glaciers and the landscape have been invaluable in shaping my understanding of the region. I recognize that significant traditional knowledge exists within the community about glacier movement and history. Much more is to be learned from this knowledge, and I am committed to continuing these conversations as my research evolves.

This thesis would not have been possible without the guidance and mentorship of my supervisors, Dr. Luke Copland and Dr. Karen Alley. Thank you both for the exceptional opportunities you have provided, your unwavering support, and for helping me grow not only as a researcher but as a person. I would also like to thank my committee members, Dr. Anders Knudby and Dr. Charles Brunette, for their thoughtful feedback and expertise.

I gratefully acknowledge the support of the University of Ottawa Department of Geography, Environment and Geomatics, la Fondation Baxter et Alma Ricard, the Natural Sciences and Engineering Research Council of Canada, the Polar Continental Shelf Program, the Northern Scientific Training Program, the Canada Foundation for Innovation, and the Department of Fisheries and Oceans Canada. Thank you to the members of the Laboratory for Cryospheric Research for the shared trauma bonding, adventures, and support over these past years.

I am grateful for the training and networking opportunities received through courses at the University of Ottawa, the University of Manitoba, the University Centre in Svalbard, and participation in conferences such as ArcticNet and the IASC Network on Arctic Glaciology.

Finally, a heartfelt thanks to my parents, sister, and friends for their endless encouragement and belief in me. To my soccer community, thank you for keeping me sane and reminding me there's a world outside of glaciers. The experiences and memories made over these past two years have shaped me profoundly and will continue to guide my future.

Preface

This thesis follows a hybrid structure and was completed under the supervision of Dr. Luke Copland (University of Ottawa) and Dr. Karen Alley (University of Manitoba). Chapter 1 establishes the scientific context through a literature review and outlines the research objectives of the project. The core research is presented in Chapter 2 as a standalone manuscript, with all references compiled in Chapter 3. Figures and tables appear alongside their relevant content throughout the text.

Prior to submission to a peer-reviewed journal such as *Journal of Glaciology*, Chapter 2 will be revised to conform to journal formatting standards and reviewed by all co-authors. The manuscript's proposed title and authorship are as follows:

Huot, D., Copland, L., Alley, K., Gervais, P. (in prep). Multidecadal Evolution in Velocity and Ice Thickness of Illaulittuuq (Coronation) and Maattatujana (Maktak) Glaciers, Baffin Island, Nunavut.

As the primary author, I led all aspects of data processing, analysis, interpretation, and manuscript writing, and participated in fieldwork including equipment deployment and in situ data collection. Dr. Luke Copland and Dr. Karen Alley each contributed guidance and feedback at all stages of the project, from initial planning through to data collection, analysis, and writing. Pénélope Gervais, a PhD candidate (University of Ottawa), supported field work and logistics, participated in data collection, and offered input on data processing.

While all work produced is original, I declare having used Claude Code artificial intelligence to help with coding aspects of my thesis such as code to make plots, to process satellite data, or to help manipulate digital elevation models in ArcGIS Pro, QGIS, and in Jupyter Notebook. As for the writing process, since I express myself better in French, I wrote some sections in French and used tools such as Antidote, Grammarly, and DeepL to help me translate content to English or refine sentence structure and vocabulary. All other works remain my own, and incorporate feedback provided by my supervisors.

Table of Contents

List of Figures

List of Tables

Abbreviations

a^{-1}	Per year
a.s.l.	Above sea level
ArcticDEM	Arctic Digital Elevation Model
ASTER	Advanced Spaceborne Thermal Emission and Reflection Radiometer
AutoRIFT	Autonomous Repeat Image Feature Tracking
CAA	Canadian Arctic Archipelago
CGVD2013	Canadian Geodetic Vertical Datum of 2013
CSRS-PPP	Canadian Spatial Reference System - Precise Point Positioning
DEM	Digital Elevation Model
DJF	December-January-February
ELA	Equilibrium Line Altitude
EPSG	European Petroleum Survey Group geodetic parameter dataset
ERA5	ECMWF Reanalysis version 5
GCP	Ground Control Point
GNSS	Global Navigation Satellite System
GVT	Glacier Velocity Tracker
HyP3	Hybrid Pluggable Processing Pipeline (HyP3)
InSAR	Interferometric Synthetic Aperture Radar
IPCC	Intergovernmental Panel on Climate Change
ITS_LIVE	Inter-Mission Time Series of Land Ice Velocity and Elevation
JJA	June-July-August
MAM	March-April-May
NAD83	North American Datum of 1983
NASA	National Aeronautics and Space Administration
NRCan	Natural Resources Canada
PPP	Precise Point Positioning
RGI	Randolph Glacier Inventory
RINEX	Receiver Independent Exchange Format
SAR	Synthetic Aperture Radar
SETSM	Surface Extraction with TIN-based Search-space Minimization
SfM	Structure from Motion
SfM-MVS	Structure-from-Motion Photogrammetry and Multi-View Stereo
SLR	Sea-Level Rise
SON	September-October-November
UBX	u-blox binary format
UTM	Universal Transverse Mercator
WGS 84	World Geodetic System 1984
WV	WorldView Satellite
w.e.	Water equivalent

Chapter 1: Background and Research Objectives

1.1. Glacier Changes

1.1.1. Global Glacier Changes

Global surface temperatures have risen by 0.06°C per decade since 1982 (NOAA National Centers for Environmental information, 2024), with 2015-2025 being the warmest years on record (World Meteorological Organization, 2025). More significantly, between the time periods 2000-2010 and 2010-2020, mean annual 2 m air temperatures at glacier termini increased by 1.99°C (Hersbach and others, 2019), and mean annual surface ocean temperatures rose by 0.23°C (Zuo and others, 2019). These changes coincide with significant global temperature anomalies, varying precipitation patterns, and extreme weather events (IPCC, 2023a). Northern regions are experiencing faster warming rates than the global average, with various studies reporting rates over different periods and definitions of the Arctic that are almost twice (Yu and others, 2021), about twice (Walsh, 2014), more than twice (Jansen and others, 2020), or four times higher (Rantanen and others, 2022).

Climate models (Noël and others, 2018), remote sensing measurements (Gardner and others, 2013; Wouters and others, 2019; Ciracì and others, 2020), and in situ observations (Gardner and others, 2013; Zemp and others, 2019) all indicate significant mass loss from the world's ice sheets, ice caps, and glaciers due to global warming. These widespread losses over the past two decades can be largely attributed to the warming pan-Arctic climate and the warming of the oceans (Zemp and others, 2015; Kochtitzky and Copland, 2022; IPCC, 2023).

Since 2000, increasingly negative cumulative and annual glacier mass balance rates have been observed globally (World Glacier Monitoring Service, 2023), including a marked acceleration in mass loss for glaciers outside the Greenland and Antarctic ice sheets (Hugonnet and others, 2021). Recently, the CAA (Canadian Arctic Archipelago) and Alaska-Yukon regions have exhibited the most significant annual mass loss rates globally, of 72.5 ± 8 Gt a^{-1} and 73.0 ± 9 Gt a^{-1}, respectively between 2002-2019 (Ciracì and others, 2020). Between 2000 and 2020, the retreat of glacier termini in regions including Russia, Northern Canadian Arctic, Svalbard, Greenland, and Alaska accounted for 50.1% of mass loss from marine-terminating glaciers in the Northern Hemisphere (Kochtitzky and Copland, 2022). Trends relating to increased thinning rates have been particularly pronounced at low elevations, particularly in the Arctic (e.g., Abdalati and others, 2004; Schaffer and others, 2020; Curley and others, 2021; Medrzycka and others, 2023).

Due to increased thinning, glaciers and ice caps outside of the major ice sheets have been a substantial contributor to 21st-century sea-level rise (SLR) (Ciracì and others, 2020). Recent geodetic mass balance studies indicate a doubling of mass loss from these glaciers, contributing 0.74 ± 0.04 mm a^{-1} to SLR between 2000 and 2019 (Hugonnet and others, 2021). Arctic land ice has been a major contributor to eustatic SLR, accounting for 31% of observed SLR from 1992-2017 (Box and others, 2018). The Intergovernmental Panel on Climate Change (IPCC) Special Report on the Ocean and Cryosphere in a Changing Climate notes a threefold increase in the rate of SLR contribution from Arctic land ice between 1986-2005 and 2006-2015 (IPCC, 2019). Under IPCC scenarios projecting a +2°C mean temperature increase between 2015 and 2100, Alaska, Greenland, Northern Canadian Arctic, and Southern Canadian Arctic are projected to contribute ~22%, 12%, 10%, and 9%, respectively, to the anticipated 99 mm of global SLR (Rounce and others, 2023).

1.1.2. Canadian Arctic Archipelago Changes

Amplified warming has led to near-surface air temperature increases of ∼1.1°C over the past two decades in the CAA, which is closely linked to the formation of high-pressure ridges over the Eastern CAA in summer, promoting warm air influx into the Western Arctic (Noël and others, 2018). Since 1996, Noël and others also note faster warming in the Northern CAA than the Southern CAA (Fig. 1), at rates of $+0.10 \pm 0.04$°C and $+0.06 \pm 0.03$°C a^{-1}, respectively. Elevation-dependent warming is also present in the Canadian High Arctic, with elevations above 1400 m a.s.l. (above sea level) experiencing warming rates more than twice those below 1000 m (Mortimer and others, 2016).

Recent climate warming trends have resulted in Canadian Arctic ice caps experiencing mass loss at a rate unprecedented in the last 4000 years (Fisher and others, 2011). Van Wychen and others (2020a) show that the mass balance of CAA's glaciers and ice caps was generally stable until the late 1980s, but saw significant losses by the mid-1990s. Thomson and others (2017) similarly report substantial losses from long-term in situ mass balance measurements in northern Nunavut, spanning from 1960 to 2014. From 2003 to 2010, CAA glaciers became the largest source of global glacier mass loss outside Greenland and Antarctica, with losses of 67 ± 6 Gt a^{-1} (Jacob and others, 2012), more than double the losses from 1995-2000 (Abdalati and others, 2004).

Observed glacier mass losses in the CAA have been mainly attributed to enhanced summer temperatures (Gardner and others, 2012) and greater meltwater runoff (Gardner and others, 2011; Sharp and others, 2011; Noël and others, 2018), rather than increased calving activity (Sharp and others, 2011; Van Wychen and others, 2014) or precipitation (Gardner and others, 2012). Despite continued mass loss trends since 2010 (Harig and Simons, 2016; Ciracì and others, 2020), some positive mass balance years have occurred due to decreased surface melt from persistent cold air anomalies (Sharp and others, 2015; Box and Sharp, 2017). Continuous monitoring of ice mass changes in the CAA is vital as projections suggest sustained and irreversible losses under moderate climate warming scenarios. Mass balance projections anticipate an increase in glacier mass losses in the CAA from 51 ± 26 Gt a^{-1} in 2000-2011 to 144 ± 33 Gt a^{-1} by 2100 (Marzeion and others, 2012; Lenaerts and others, 2013).

Glacier thinning patterns in the CAA as a whole varies with elevation, showing pronounced thinning below 1600 m (Abdalati and others, 2004). Marine-terminating glaciers in the northern CAA, often grounded below sea level, are especially vulnerable to thinning from SLR and warm ocean waters (Van Wychen, and others, 2020a; Dalton and others, 2022). The CAA's accelerated mass loss, particularly since 2005 (Gardner and others, 2011; Millan and others, 2017; Noël and others, 2018), explains how these glaciers emerged as the largest non-continental ice sheet contributors to SLR by the 2000s (Box and others, 2018; Gardner and others, 2012; Van Wychen, and others, 2020a). Canada's glaciers and ice caps have recently contributed 0.16 mm a^{-1} to global SLR, equivalent to 23% of Greenland's and 75% of Antarctica's contributions (Shepherd and others, 2012; Gardner and others, 2013).

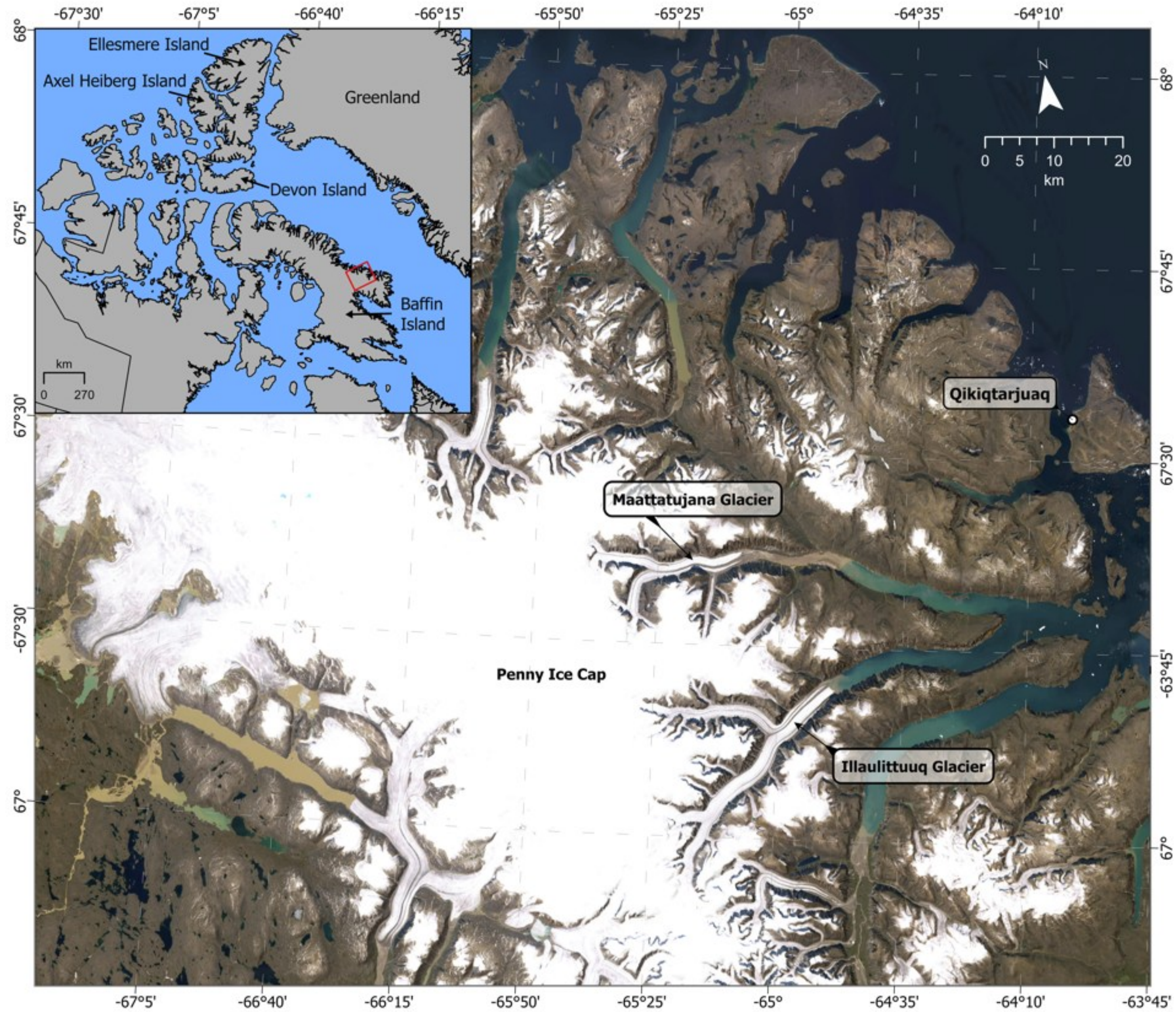

Figure 1. Overview of the study area, highlighting Illaulittuuq and Maattatujana glaciers, Penny Ice Cap, and the community of Qikiqtarjuaq on Baffin Island. Inset shows the location within the Canadian Arctic Archipelago (CAA), with major islands of the northern CAA (Ellesmere, Axel Heiberg, Devon Island) and southern CAA (Baffin Island) labelled.

1.2. Glacier Dynamics

1.2.1. Mass Change of Land vs. Marine-Terminating Glaciers

Land-terminating glaciers undergo volume changes influenced by two main feedback processes: a positive feedback tied to surface elevation loss, and a negative feedback related to glacier length. As the glacier's surface lowers due to decreased mass balance, a higher percentage of the glacier area falls within the ablation zone, the portion of the glacier where annual mass loss (through melt, sublimation, and calving) exceeds mass gain, resulting in a net negative mass balance. This expansion of the ablation area accelerates terminus retreat and mass loss. However, this retreat simultaneously stabilizes the mass loss as the ablation area found at the lowest and warmest elevations reduces as the terminus retreats.

Marine-terminating glaciers exhibit feedback loops similar to land-terminating glaciers, as well as additional mechanisms such as the tidewater glacier cycle, even in stable climates (Amundson, 2016). According to Brinkerhoff and others (2017), the tidewater glacier cycle begins with a gradual ice advance under positive mass balance conditions and sediment shoal buildup, shielding the glacier from frontal ablation. As the glacier reaches an unstable equilibrium with near-neutral mass balance, even slight increases in mass loss (due to external forcings or internal changes in the supply of ice and sediment to the terminus) trigger retreat. If the glacier bed slopes downward (retrograde slope) in the direction of retreat, this retreat progresses into deeper water, which can accelerate flow, cause dynamic thinning, or increase calving due to reduced basal and lateral resistance. Retreat continues until the terminus reaches bed elevations near sea level or encounters topographic constraints. Once stabilized, slow glacial advance resumes, influenced by terminal moraines, varying ice flow, subglacial topography, and sediment supply (Amundson, 2016; Truffer and Motyka, 2016). Compared to land-terminating glaciers, marine-terminating glaciers exhibit more pronounced mass loss mechanisms, primarily through frontal ablation, and are highly responsive to climate and ocean conditions such as water motion, salinity, depth, and water temperature (Truffer and Motyka, 2016). Consequently, they often experience faster mass loss and terminus retreat.

Despite marine-terminating glaciers constituting 40% of Earth's ice masses outside the ice sheets, they only contribute 26% to global glacier mass losses (Hugonnet and others, 2021). Between 2000 and 2020, 85.3% of Northern Hemisphere glaciers reaching the ocean were retreating, 2.5% were advancing, and 12.3% remained unchanged (Kochtitzky and Copland, 2022). While a delayed response to climate changes (Larsen and others, 2015) may, in part, explain the smaller mass loss of marine-terminating glaciers, both glacier types exhibit similar accelerated losses within Arctic regions (Hugonnet and others, 2021). Moreover, Cook and others (2019) found little evidence of ocean temperatures driving long-term retreat patterns in the CAA's marine-terminating glaciers, which flow into shallow water, limiting ocean influence. Instead, they suggest that increased surface air temperatures are the primary driver of retreat for most marine-terminating glaciers in the CAA, similar to land-terminating glaciers. This corroborates Van Wychen and others (2014), who found that only about 7.5% of glacier mass losses in the Canadian Arctic are due to calving.

1.2.2. Glacier motion

Glacier motion results from the balance between gravitational driving stresses and resistive forces acting within the ice and at its base (Weertman, 1957; Glen, 1958; Jiskoot, 2011). The resulting ice velocity reflects the combined contributions of internal deformation, basal sliding, and, where applicable, deformation of subglacial sediments, with the relative importance of each mechanism controlled by ice geometry, basal conditions, and subglacial water pressure.

1.2.2.1 Internal Deformation

Internal deformation represents the viscous flow of glacier ice driven by gravitational stresses associated with ice thickness and surface slope (Jiskoot, 2011; Paterson, 1994). Under sustained stress conditions typical of glacier interiors, ice deforms plastically over time rather than fracturing. Glacier ice deforms according to a non-linear relationship between applied stress and strain rate, commonly described by Glen's flow law (Glen, 1958), in which strain rate increases as a power-law function of applied stress. The flow parameter is strongly temperature dependent and influenced by temperature, ice fabric (the crystallographic orientation of ice crystals, which affects the ease of internal slip), and impurity content (Paterson, 1994).

Although Glen's flow law provides a practical constitutive framework for describing ice creep, it incorporates several simplifying assumptions. The law is derived for simple shear, whereas natural glacier flow involves multi-directional stress fields, such that deformation in any one direction may be lower than predicted by simple shear alone (Paterson, 1994). In addition, glacier ice is neither perfectly homogeneous nor isotropic; the development of preferred crystal orientations, particularly near the bed, can locally enhance deformability beyond that predicted by isotropic rheology (Hubbard and Sharp, 1995). Despite these limitations, internal deformation is generally treated as a relatively smooth and slowly varying component of glacier motion that responds primarily to long-term changes in thickness and surface slope.

1.2.2.2 Basal Sliding

Basal sliding occurs when glacier ice at the pressure-melting point moves relative to its bed, adding to glacier motion caused by internal deformation. Two general sliding processes are typically recognized in the literature, distinguished by whether the ice remains in continuous contact with the bed or becomes partly separated from it as basal water pressure increases (Weertman, 1957; Lliboutry, 1968; Jiskoot, 2011).

The first process operates when the ice remains in contact with the bed. In this case, sliding is enabled by ice motion around bedrock irregularities through a combination of enhanced creep and regelation. Enhanced creep results from locally elevated stresses around bed obstacles that promote viscous deformation of ice, while regelation involves pressure-induced melting on the upstream sides of obstacles and refreezing on the downstream sides. The efficiency of these processes depends on the scale of bed roughness, with small-scale features favouring regelation and larger features favouring enhanced creep (Weertman, 1957).

The second process becomes important when basal water pressure is sufficiently high, or sliding is sufficiently fast, to allow cavities to form on the downstream sides of bedrock obstacles, leading to partial separation between the ice and the bed. Under these conditions, sliding velocity is strongly influenced by effective pressure, defined as the difference between ice overburden pressure and basal water pressure (Iken, 1981). Changes in the structure of the subglacial drainage system can therefore produce marked temporal variations in sliding speed, particularly where transitions occur between efficient channelized drainage and more distributed drainage configurations (Kamb, 1987; Jiskoot, 2011). As a result, basal sliding is widely regarded as a primary control on short-term and seasonal variability in glacier velocity (Willis, 1995).

1.2.2.3 Subglacial Bed Deformation

Where glaciers rest on unconsolidated, water-saturated sediments, basal motion may also be accommodated through deformation of subglacial till (Truffer and others, 2000). In such settings, some or all of the basal shear stress can be taken up within the sediment layer once applied stresses exceed the yield strength of the till, rather than being transmitted entirely through sliding at the ice-bed interface (Alley and others, 1986; Boulton and Hindmarsh, 1987). The mechanical behaviour of subglacial till is strongly influenced by pore-water pressure, grain size distribution, and sediment structure, with high water pressures reducing effective stress and promoting deformation at relatively low basal shear stresses (Alley and others, 1986).

Observations from instrumented glacier beds show that subglacial sediment deformation is often spatially heterogeneous rather than uniform (Truffer and others, 2000). Deformation may occur within thin shear zones near the ice-sediment interface, be distributed through a thicker sediment layer, or be localized along internal sediment boundaries, depending on sediment properties and basal hydrological conditions (Truffer and Motyka, 2016). Because sediment strength and pore-water pressure vary in space and time, subglacial bed deformation remains challenging to define with a single constitutive law (Zoet and Iverson, 2020). Basal motion over soft beds is commonly shared between sediment deformation and basal sliding, with the relative contribution of each varying in response to changes in basal water pressure and sediment conditions (Boulton and Hindmarsh, 1987; Alley, 2000; Truffer and Motyka, 2016).

1.3 Glacier Measurements

1.3.1. Geodetic Mass Balance

Mass balance, a key method for analyzing global glacier changes (Zemp and others, 2013a; Ciracì and others, 2020; Hugonnet and others, 2021; Schaffer and others, 2023), measures seasonal to decadal glacier mass gains or losses (Cogley and others, 2011). As a measure that reflects atmospheric forcing and, in the case of marine-terminating glaciers, oceanic conditions, it serves as a critical indicator of climate change, sea-level rise, and local glacial and hydrological impacts (Braithwaite and Hughes, 2020).

While in situ, gravimetric, and laser altimetry methods (Gardner and others, 2013) can determine mass balance, geodetic methods are popular and accurate for monitoring glacier mass changes over years to decades (Cogley, 2009; Gardelle and others, 2012; Schaffer and others, 2020). Although surface mass balance processes dominate changes in locations such as Alaska and the CAA (Larsen and others, 2015; Millan and others, 2017), geodetic methods, which account for surface, internal, and basal balances, provide a more comprehensive approach (Zemp and others, 2013b).

Geodetic mass balance methods determine volume changes by repeatedly mapping glacier surface elevations (Cogley and others, 2011), which are typically measured using global navigation satellite systems, airborne or spaceborne photogrammetry, SAR (Synthetic Aperture Radar) interferometry (Berthier and others, 2007), or laser altimetry (Moholdt and others, 2010). Established methods for the Canadian High Arctic include using DEMs (Digital Elevation Model) derived from stereo satellite photogrammetry. Notably, strip DEMs with known dates are available from ArcticDEM (https://www.pgc.umn.edu/data/arcticdem/), and ASTER stereo imagery can be processed using the MicMac ASTER software package (Lauzon and others, 2023). Additionally, DEMs can be derived from structure-from-motion photogrammetry applied to historical and recent aerial photography (Thomson and Copland, 2016; Medrzycka and others, 2023). As part of this, co-registration techniques need to be employed to produce reliable and accurate DEMs and determine their changes over time (Thomson and Copland, 2016; Thomson and others, 2017). Surveys should also be conducted at the end of the ablation season to minimize short-term elevation fluctuations from seasonal and interannual meteorological processes and ideally repeated at least each decade (Zemp and others, 2013a).

Excluding DEM sighting errors (caused by sensor and interference of the atmosphere), and plotting errors (caused by geo-referencing, projection, co-registration, and sampling density), ice volume changes are expressed by the following equation (Zemp and others, 2013a):

$$\Delta V = r^2 \sum_{k=1}^{K} \Delta h_k, (1)$$

where K is the number of pixels covering the glacier, Δh_k is the difference in elevation between the two grids at pixel k, and r is the pixel size. The difference between DEMs from two periods provides a change in glacier volume, which is converted to mass change using a conversion factor ($f_{\Delta V}$) based on ice/firn density (Huss, 2013):

$$\Delta M = f_{\Delta V} \cdot \Delta V, (2)$$

Under Sorge's law, high polar glacier snow density is relatively invariant with time if there is no significant melting; therefore, a factor of ~900 kg m^{-3} is suggested for ice density (Bader, 1954). To better reflect regional firn conditions, certain studies have adopted a factor of 850 kg m^{-3} (Sapiano and others, 1998; Thomson and others, 2017), although some studies prefer zonally variable conversion factors based on in-situ measurements (e.g., Schaffer and others, 2020). Despite challenges in determining an accurate factor, Huss (2013) recommends 850 ±60 kg m^{-3} to account for densification, internal refreezing, and firn volume changes. Huss' value is recommended for geodetic observations over periods longer than 5 years on glaciers with stable mass balance gradients and firn regions. For shorter intervals (≤3 years), the conversion factor may vary significantly; therefore caution is required, especially without in-situ density data.

1.3.2. Glacier Velocities

An important question in evaluating Arctic glaciers' response to climate change is how glacier flow speeds change as mass is lost, as observed velocity responses are highly variable and warrant investigation across longer temporal scales to develop our understanding of regional trends (Schaffer and others, 2017). Decadal analyses have shown reduced velocities of non-surging, land-terminating glaciers with increasingly negative mass balances in Patagonia, Pamir, Caucasus, Alaska Range (Heid and Kääb, 2012), Yukon (Main and others, 2023), Southern CAA (Schaffer and others, 2017), and Northern CAA (Thomson and Copland, 2017b). This velocity reduction may be due to increased surface melt enhancing the formation of efficient channelized subglacial drainage systems (Schaffer and others, 2017; Thomson and Copland, 2017a), and/or thinner ice caused by enhanced melt or decreased mass accumulation, leading to reduced driving stress (Heid and Kääb, 2012; Main and others, 2023; Schaffer and others, 2017; Thomson and Copland, 2017b). However, there is no clear correlation between regional mass balance magnitude and long-term speed change, due to varying response times, non-representative data regions, and independent changes in water pressure or surge-type activities. Conversely, while acceleration is mainly associated with positive mass balance conditions (Anderson and others, 2014), some non-surge-type marine-terminating glaciers have been accelerating over recent decades in the Northern CAA (Van Wychen and others, 2016, 2020b), such as Trinity and Wykeham glaciers on South East Ellesmere Island (Dalton and others, 2022).

Velocity patterns also vary between glacier types, with larger marine-terminating glaciers typically showing continuous speed increases up to the ice front, while land-terminating glaciers (Millan and others, 2017) and smaller marine-terminating glaciers, such as those in the Southern CAA (Van Wychen and others, 2015), often have their highest speeds near the equilibrium line altitude and are relatively stagnant at the terminus. Additionally, Van Wychen and others (2017, 2020b) quantify how glaciers with beds below sea level exhibit greater velocity variability compared to those whose beds are above sea level. Differences in velocity patterns from the upper glacier to the terminus, when comparing Northern and Southern CAA glaciers, are generally attributed to larger accumulation zones that sustain flow in northern glaciers, along with variations in basal friction between marine termini in the north and land-terminating termini in the south (Van Wychen and others, 2015).

With our growing understanding of glacier velocities, various methods are readily employed to measure these fluctuations. SAR imagery is particularly effective due to its ability to operate in nearly all weather conditions, particularly in the winter, unlike optical methods. However, optical techniques can often work better in the summer under high melt conditions, and can offer higher spatial resolution in regions with distinct surface features, providing more accurate measurements where conditions allow (Huang and Li, 2011).

Techniques such as interferometry (InSAR) (Burgess and others, 2005; Lauzon and others, 2023) and speckle tracking (Van Wychen and others, 2012; Millan and others, 2017) have shown success in measuring glacier velocities from SAR imagery across the Canadian Arctic. These methods derive glacier velocities from total displacement, considering both azimuthal and range displacements (Van Wychen and others, 2015; Lauzon and others, 2023).

Glacier velocity tracking in the Canadian High Arctic was significantly enhanced by the launch of the RADARSAT-2 satellite in 2007 and further improved by the RADARSAT Constellation Mission in 2017, which advanced regional-scale observations and speckle tracking methods (Schaffer and others, 2017; Van Wychen and others, 2020a). Feature tracking methods applied to optical (and radar) imagery have been further advanced through NASA's Inter-mission Time Series of Land Ice Velocity and Elevation (ITS_LIVE v2.0) dataset (Gardner and others, 2025). ITS_LIVE v2.0 provides image pair velocity records from 1982 to present, processed in near-real time after new satellite image acquisitions. ITS_LIVE products have become a main source for high-resolution velocity data notably in the Canadian Arctic (e.g., Lauzon and others, 2023). This data also allows quantification of the importance of intra-annual and seasonal variability in glacier velocities and their response to environmental changes (Greene and Gardner, 2025).

1.4 Research Objectives

Within the context of how we study glacier change over time, the primary objective of this thesis is to quantify the patterns and processes underlying glacier changes on southern Baffin Island in response to a warming climate. This is undertaken by studying Illaulittuuq and Maattatujana glaciers, two of the largest outlet glaciers of Penny Ice Cap, from 1958-2024. This thesis will:

(1) Outline terminus retreat and frontal ice loss using historical air photos and optical satellite imagery.

(2) Determine seasonal and yearly velocity changes through feature tracking of historical air photos and optical satellite imagery, including Landsat 1-9 and Sentinel-2.

(3) Quantify geodetic mass balance (i.e., changes in ice thickness and mass) using modern digital elevation models, complemented by structure-from-motion photogrammetry and multi-view stereo (SfM-MVS) processing applied to historical aerial photography to derive historical DEMs.

(4) Conduct a comparative analysis between Illaulittuuq Glacier (marine-terminating) and Maattatujana Glacier (land-terminating) to understand the processes driving their observed changes and to evaluate whether terminus type is a significant factor in this.

This project also forms part of a broader initiative supported by the Department of Fisheries and Oceans to address the community of Qikiqtarjuaq's concerns about local ecosystems and coastal changes. While the direct linkages between glacier change and downstream ecosystem or community impacts are not investigated within this thesis, this research contributes a necessary foundation for future work addressing those questions. Quantifying the velocity, thickness, and mass balance changes of Illaulittuuq and Maattatujana glaciers provides essential baseline information for understanding how these glaciers influence fjord conditions, particularly through freshwater discharge and sediment output. These outputs shape fjord water properties, including stratification, turbidity, and nutrient availability, which in turn influence local marine ecosystems and the fisheries and wildlife on which the Qikiqtarjuaq community depends. As such, the glaciological findings presented here are intended to support subsequent, more targeted investigations into the connections between glacier change, fjord dynamics, and community and ecosystem impacts in the region.

Chapter 2: Assessing Evolving Glacier Dynamics of Illaulittuuq and Maattatujana Glaciers from 1958-2024

2.1 Introduction

Glacial mass loss in the Canadian Arctic Archipelago (CAA) has accelerated significantly in recent years (Hugonnet and others, 2021). Losses have been particularly important in southerly parts of the CAA, including Nunavut's Baffin Island, where area-averaged mass loss rates were double those of the northern CAA during 2003-2009 (Gardner and others, 2013). This mass loss was driven by a warming of ~10°C in near-surface firn temperatures between the mid-1990s and 2011 (Zdanowicz and others, 2012), which brought melt rates to their highest level in the past 4000 years (Fisher and others, 2011). Within southern Baffin Island, Penny Ice Cap exemplifies these changes, having had a negative mass balance since the mid-1990s, with losses of 1.3 ± 0.7 Gt a^{-1} from 1995-2000 (Abdalati and others, 2004) and 2.9 ± 1.1 Gt a^{-1} from 2000-2005 (Gardner and others, 2012), followed by losses of 5.4 ± 1.9 Gt a^{-1} up to 2014 (Schaffer and others, 2020, 2023).

This mass loss, primarily driven by atmospheric warming, has led to rapid ice thinning at low elevations and to substantial terminus retreat across both land- and marine-terminating outlet glaciers of Penny Ice Cap (Hugonnet and others, 2021). Notably, Illaulittuuq Glacier (Coronation Glacier; marine-terminating) and Maattatujana Glacier (Maktak Glacier; land-terminating) retreated by approximately 820 m and 380 m, respectively, between 1985 and 2011 (Schaffer and others, 2017). This terminus retreat and associated mass loss have been accompanied by dynamic adjustments in ice flow. While an overall deceleration has been reported over the 1985-2010 period (Heid and Kääb, 2012), Schaffer and others (2017) revealed a more complex pattern, with an initial phase of acceleration through the late 1990s, which preceded a longer-term slowdown that persisted through at least 2014. While the magnitude and timing of these changes vary between the two glaciers, their surface velocity patterns are consistent with those observed at other southern CAA outlet glaciers (Van Wychen and others, 2015). Both glaciers exhibit along-glacier transitions between motion dominated by ice deformation, regions of enhanced basal sliding, and restricted flow zones with increased basal friction (Van Wychen and others, 2020b); however, the overall reduction in ice motion is hypothesized to reflect a longer-term shift from basal-sliding-dominated flow toward motion being increasingly governed by internal deformation as glacier thinning progresses (Schaffer and others, 2017). Together, these increases in mass loss, terminus retreat patterns and changes in velocity highlight the influence of a warming climate across Penny Ice Cap's outlet glaciers.

Despite advances in knowledge of decadal-scale glacier mass balance and velocity changes on Penny Ice Cap (e.g., Heid and Kääb, 2012; Schaffer and others, 2017; Noël and others, 2018; Van Wychen and others, 2020b), recent changes remain poorly constrained. Current velocity records mainly end around 2014, and have not used new, more accurate datasets. In addition, the coupling of long-term mass loss and seasonal to interannual variations in ice flow remains insufficiently characterized, limiting our ability to determine whether observed velocity changes reflect a sustained dynamic response to ice thinning, or variability driven by meltwater availability and evolving basal conditions. Given the pronounced sensitivity of glaciers in the southern Canadian Arctic Archipelago, including Penny Ice Cap, to recent climate forcing (Rodríguez-Cuicas and others, 2023), and projections indicating that future mass losses on Penny Ice Cap will be concentrated at low elevations (Schaffer and others, 2023), understanding the evolution of Penny Ice Cap's outlet glaciers is critical for assessing future ice discharge and dynamic changes under continued atmospheric warming.

To provide a comprehensive multi-decadal assessment of ice velocity, mass balance, and terminus retreat across Penny Ice Cap's eastern margin, this study focuses on Illaulittuuq and Maattatujana glaciers, two neighbouring outlet glaciers exposed to a similar regional climate but characterized by contrasting terminus types. This comparative approach enables evaluation of whether the evolving dynamic behaviour of these glaciers aligns more closely with land- or marine-terminating glacier responses described elsewhere. Beyond advancing understanding of glacier dynamics in the southern Canadian Arctic, these changes also have important environmental implications, as retreating outlet glaciers on Penny Ice Cap regulate freshwater, sediment, and iceberg fluxes to adjacent fiords, influencing coastal ecosystems that are vital to local Inuit communities (Bhatia and others, 2021), as well as impacting sea-level rise (IPCC, 2023b). In this context, this study has been undertaken in partnership with the Department of Fisheries and Oceans Canada and the community of Qikiqtarjuaq, supporting efforts to assess the ecological consequences of ongoing glacier retreat and providing the glaciological baseline needed to inform that broader assessment.

2.2 Study Area

2.2.1 Penny Ice Cap

Penny Ice Cap, situated along the mountainous eastern margin of Baffin Island, forms one of the largest ice masses in the southern Canadian Arctic (Fig. 1). Icefields and ice caps occupy roughly 23,600 km² within 100 km of Baffin Island's coastline (Gardner and others, 2012), with Penny Ice Cap (6,410 km²) and Barnes Ice Cap (5,900 km²) representing two important remnants of the Laurentide Ice Sheet (Zdanowicz and others, 2002; Zdanowicz and others, 2012). Penny Ice Cap rises to approximately 1,930 m a.s.l. and reaches a maximum thickness of ~880 m (Shi and others, 2010; Zdanowicz and others, 2012), with its surface morphology marked by a broad, gently sloping western dome and steeply incised outlet glaciers along the remaining margins.

Penny Ice Cap is drained by a combination of many land-terminating glaciers and two marine-terminating glaciers, all of which are non-surge-type (Van Wychen and others, 2015). Ice flow within the ice cap interior is slow (<20 m a^{-1}), increasing to ~100-250 m a^{-1} along the upper trunks of the outlet glaciers (Van Wychen and others, 2015; Schaffer and others, 2017). Mass balance observations from 2006-2014 indicate an average equilibrium line altitude of ~1646 m (ranging between 1320 and 1820 m) and a strongly negative mean surface mass balance of -1.2 m w.e. a^{-1} (Schaffer and others, 2023). Thinning at the margins reaches 3-4 m a^{-1}, among the highest rates documented in the Canadian Arctic Archipelago (Fisher and others, 2011; Zdanowicz and others, 2012).

In recent decades, sustained atmospheric warming has driven substantial changes in both the extent and surface properties of Penny Ice Cap. The ice cap experienced an area reduction of approximately 452 ±227 km² (6.6%) between 1985-1989 and 2019-2021 (Ali and others, 2023), reflecting the broader pattern of glacier retreat observed across the Arctic. In parallel, the melt season length nearly doubled between 1979 and 2010, promoting deeper meltwater percolation, firn densification, and an increase of approximately 10°C in 10 m firn temperatures by 2011 (Zdanowicz and others, 2012). If the ongoing warming trend continues, Penny Ice Cap is projected to lose its firn zone within the next several decades, transitioning first toward superimposed ice and becoming effectively firn-free by 2100 (Schaffer and others, 2023). A firn-free glacier surface refers to conditions where the intermediate, porous snow layer that normally stores meltwater has disappeared, resulting in a predominantly bare ice or impermeable ice surface with reduced capacity to retain meltwater.

2.2.2 Illaulittuuq and Maattatujana Glaciers

This study examines examples of two primary outlet glacier types on Penny Ice Cap: Illaulittuuq (Coronation) Glacier, the largest marine-terminating outlet, which flows into Illaulittuuq Fiord, and Maattatujana (Maktak) Glacier, a land-terminating glacier, located about 25 km to the north towards Maattatujana Fiord (Figs. 1 and 2). Their respective fiords attain maximum depths of 685 m and 565 m (Syvitski and others, 2022), and both lie within the Broughton Trough system that channels meltwater and sediment toward Baffin Bay.

Limited previous work has been undertaken on these glaciers, and Maattatujana Glacier remains particularly understudied (Heid and Kääb, 2012; Schaffer and others, 2017; Van Wychen and others, 2020; Rodríguez-Cuicas and others, 2023). Long-term context provided by sediment cores taken in Illaulittuuq Fiord indicate that Illaulittuuq Glacier's retreat has accelerated under climate warming since approximately 1850 CE (Rodríguez-Cuicas and others, 2023). Modern velocity records are limited to the period 1985-2014, during which time Schaffer and others (2017) showed that Maattatujana Glacier shifted from relatively high velocities in the late 1980s and 1990s to slower flow thereafter. Illaulittuuq Glacier displayed a somewhat similar pattern about 25 km up-glacier from the terminus, although its lower trunk behaved differently: velocities decreased between 5 and 25 km from the terminus during 1985-2014, but increased within 5 km of the terminus after 1998. Historically, Illaulittuuq Glacier has also been one of Penny Ice Cap's major contributors to iceberg discharge, releasing ~9.3 Mt a^{-1} in 2011 (Van Wychen and others, 2015).

Illaulittuuq and Maattatujana glaciers lie within 60 km of the Inuit community of Qikiqtarjuaq, home to ~600 residents (Statistics Canada, 2017). Community members have expressed growing concern about rapid changes to local glaciers and fiords due to their potential impacts on wildlife health, hunting access, travel safety, and regional environmental stability. The behaviours of Illaulittuuq and Maattatujana glaciers therefore have both scientific and local relevance, offering insight into how terminus setting and geometry shape differential glacier responses to modern warming.

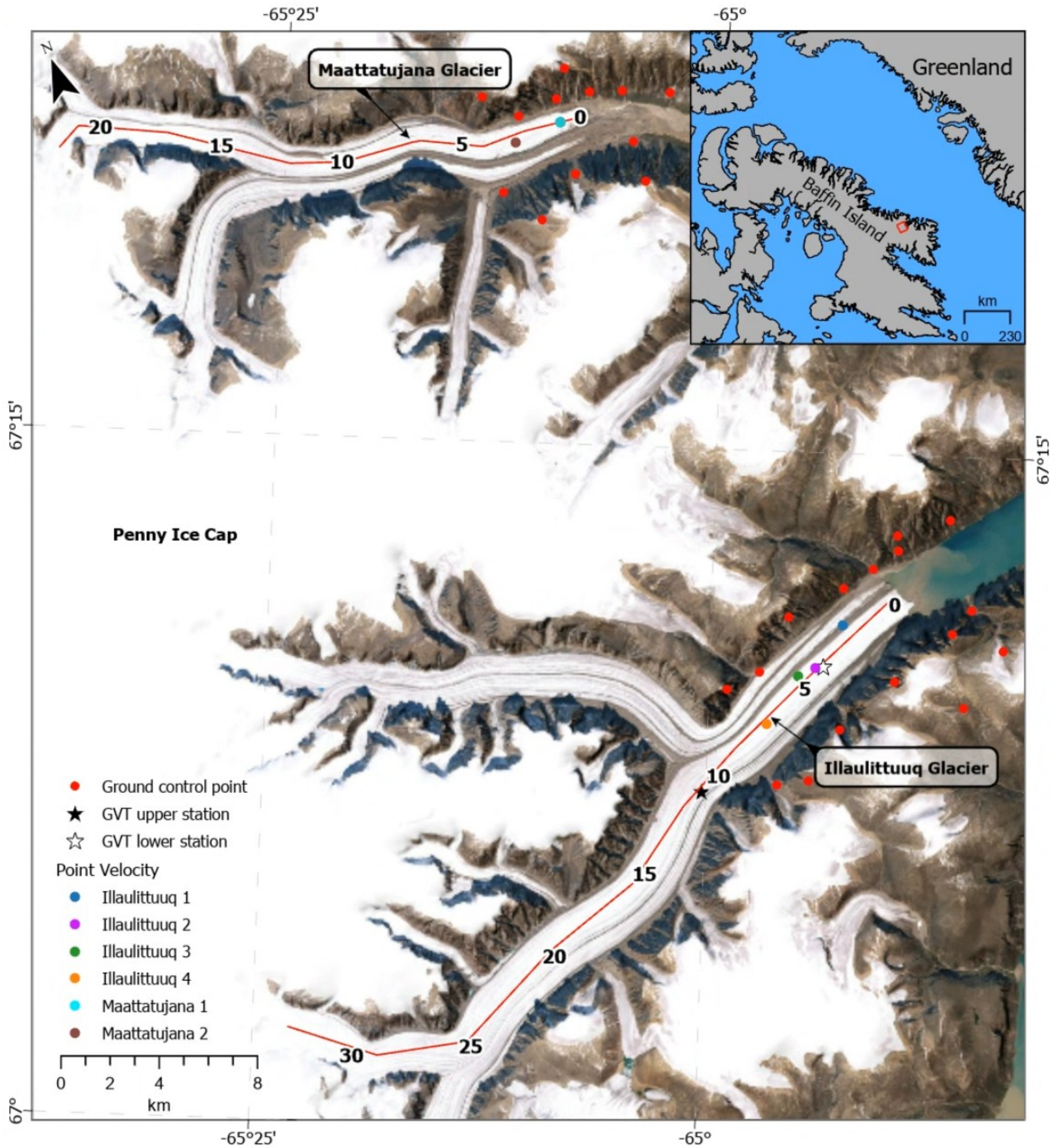

Figure 2. Penny Ice Cap on Baffin Island, Nunavut (WorldView-3: 18 July 2025), showing Illaulittuuq and Maattatujana glaciers with their respective centerlines, the locations of Glacier Velocity Tracker (GVT) stations installed in 2024, ground control points used for georeferencing historical air photos for terminus extent delineation, and the location of point velocity measurements. Data: Statistics Canada, 2021 Census - Provinces/territories - Cartographic Boundary File (https://www12.statcan.gc.ca/census-recensement/2021/geo/sip-pis/boundary-limites/index2021-eng.cfm?year=21). Natural Resources Canada - Lakes, Rivers and Glaciers in Canada - CanVec Series - Hydrographic Features (https://open.canada.ca/data/en/dataset/9d96e8c9-22fe-4ad2-b5e8-94a6991b744b).

2.3 Methods

2.3.1 Glacier Terminus Change

2.3.1.1 Terminus Position

Terminus positions and corresponding change in ice area for Illaulittuuq and Maattatujana glaciers were delineated at approximately decadal intervals from 1958 to 2024 using four historical aerial photographs and 5 optical satellite images (Table 1). To ensure consistency across the multi-decadal record, all glacier termini were manually digitized in ArcGIS Pro 3.1.0 at a consistent mapping scale to avoid resolution-dependent variations. Automated classification techniques such as the Normalized Difference Snow Index were not used to map glacier extents as relevant wavelength images are not available for historical aerial photographs and they often perform poorly in shadowed or debris-covered zones near glacier termini (Medrzycka and others, 2023).

Nadir aerial photographs from the summer of 1958 and 1975, acquired at altitudes between 22,500 ft (6858 m) and 30,080 ft (9168 m) a.s.l., were obtained from the National Air Photo Library (Ottawa, Canada). Each image was manually georeferenced in ArcGIS Pro using a first-order affine transformation to a July 1, 2025, Sentinel-2 reference scene. A minimum of 10 ground control points (GCPs) were selected on clearly distinguishable stable bedrock features at varying elevations across the study area to ensure spatial representativeness and minimize bias (Fig. 2).

Terminus positions from 1985 onward were mapped from Landsat 5/7/8, Collection 2, Level-1 TP (precision and terrain-corrected) optical satellite imagery obtained from United States Geological Survey EarthExplorer, and Sentinel-2B Level-1C optical imagery from the Copernicus Data Space Ecosystem. Only summer (June-August) acquisitions were used to minimize snow cover. These products are already radiometrically and geometrically corrected, so no further processing was required aside from projecting all datasets to WGS 84 / UTM Zone 20N (EPSG:32620).

The positional uncertainty of each terminus outline was estimated from the spatial resolution of the imagery (Table 1), combined with the horizontal offsets arising from manual georeferencing of the historical aerial photographs (Partington and others, 2025). Since the 1958 and 1975 aerial photographs required manual georeferencing, residual horizontal misalignments between these historical images and modern satellite scenes were quantified by comparing the mapped positions of stable, non-glacial terrain features against their locations in a high-resolution Sentinel-2 image acquired on July 1, 2025. These validation points were independent of the GCPs used during georeferencing to ensure that the measured offsets reflected real positional discrepancies, rather than internal fitting error.

To propagate these uncertainties into mean annual terminus-retreat rates, the additional horizontal offset associated with the historical aerial photographs was added to the pixel-resolution term in Equation (3) below. Mean horizontal offsets in the air photos were calculated from eight independent validation points, with Illaulittuuq Glacier exhibiting mean offsets of 59 m (1958-1975) and 37 m (1975-1985), whereas Maattatujana Glacier exhibited offsets of 55 m and 56 m over the same respective intervals.

Assuming all error sources are random and independent, the total uncertainty in mean annual terminus-retreat rate for each interval was computed as (Hall and others, 2003):

$$Uncertainty \; = \frac{\sqrt{(pixel\ length)^2 + (pixel\ width)^2} + \text{georectification error}}{\Delta t}, \quad (3)$$

where Δt is the time interval between successive outlines, pixel length and pixel width correspond to the mean pixel size (m) of the two images used in each interval, and the georectification error represents the measured horizontal offset (m) applied only to intervals involving historical aerial photographs.

Table 1. Imagery used for mapping the terminus positions of Illaulittuuq and Maattatujana glaciers.

Acquisition date	Image ID	Resolution (m)	Satellite/Camera	Glacier
11 June 1958	A16219-015	~0.75	RC5-311	Maattatujana
14 July 1958	A16217-009	~0.75	RC5A-311	Illaulittuuq
23 August 1975	A24200-011	~0.63	ZEISS 15/23	Maattatujana
23 August 1975	A24200-040	~0.63	ZEISS 15/23	Illaulittuuq
15 June 1985	LT05L1TP01701319850625	30	Landsat 5 TM	Both
15 August 1995	LT05L1TP01801319950815	30	Landsat 5 TM	Both
10 July 2005	LE07L1TP01701320050710	15	Landsat 7	Both
23 July 2015	LC08L1TP01601320150723	15	Landsat 8	Both
19 July 2024	MSIL1C20240719T160829	10	Sentinel 2B	Both

2.3.1.2 Terminus Area

Terminus-area change between the periods defined in Table 1 was calculated from polygons constructed between successive glacier terminus outlines. Uncertainty in these area measurements was estimated using the pixel-shift equation (4) described by Krumwiede and others (2014), which assumes that the mapped glacier boundary may be offset by ±1 pixel. The resulting area error (A_{er}) is expressed as:

$$A_{\mathrm{er}} = n \cdot m, \text{(4)}$$

where n is an estimate of how many pixels span the glacier terminus and m is the area represented by a single pixel. Uncertainties from the two outlines bounding each interval were combined in quadrature (i.e., the square root of the sum of their squared uncertainties), and the resulting value was divided by the time separation to obtain the uncertainty in mean annual area-loss rate.

2.3.2 Glacier Velocities

Centerline velocity profiles were extracted along the most dynamically active centerline flow paths of each glacier, following the approach of Schaffer and others (2023) and Van Wychen and others (2020). For Maattatujana Glacier, the centerline follows the northern arm, and for Illaulittuuq Glacier, it follows the northern branch of the southern arm (Fig. 2).

2.3.2.1 Manual Feature Tracking

Manual point surface velocities were derived from the georeferenced historical aerial photographs used for the terminus area calculations (Table 1: 1958 and 1975), and a 1974 orthophoto of Illaulittuuq Glacier used for DEM generation (see section 2.3.3.1). Respectively, for Illaulittuuq and Maattatujana glaciers, four and two locations were selected near the glacier terminus where distinct and identifiable large boulders could be recognized between images. The limited number of trackable points reflects the restricted spatial coverage of usable boulder features within the historical imagery; nonetheless, these points provide a valuable, record of surface velocity in the terminus area. For each measurement period, the horizontal displacement of selected features (following the glacier flowline) was measured between image acquisition dates in UTM Zone 20N, EPSG 32620. Surface velocity was then standardized by dividing the displacement by the time interval between observations.

To facilitate comparison with satellite-derived velocity products, the midpoint location of each manual displacement vector from the earliest measurement period (1958-1974/75) was used to extract velocity values from all available datasets and observation periods from 1958-2024 (see sections below).

2.3.2.2 Pycorr Yearly Velocities

Glacier surface velocities between 1985 and 1998 were derived from approximately yearly separated, cloud-free summer Landsat 5 Thematic Mapper Level-1 terrain-corrected imagery using the open-source feature tracking software pycorr_iceflow (v1.1; https://github.com/markf6/pycorr_iceflow). Only image pairs acquired from the same Landsat path/row were processed together to ensure consistent viewing geometry and spatial alignment (Table 2). The software first applies a high-pass filter to both images to enhance surface texture, after which a normalized cross-correlation algorithm is used to estimate pixel displacements between acquisitions. These pixel offsets are converted to ground displacement using the image spatial resolution and divided by the temporal separation between image dates to derive glacier surface velocities. To correct for systematic misregistration between image pairs, the ITS_LIVE global land mask (Gardner and others, 2025), a globally gridded product from the ITS_LIVE project classifying surface pixels as ice, land, or ocean, was used to identify stable, non-glaciated terrain, allowing median pixel offsets over land to be estimated and removed from the displacement field. The resulting velocity output excludes pixels that lack a well-defined correlation peak, that exceed the defined displacement search window of the feature-tracking algorithm (~75 pixels; ~2.25 km), or are affected by edge effects within the Pycorr workflow.

Uncertainty in the historical Pycorr-derived velocities was estimated empirically from stable, non-glaciated terrain. Using the ITS_LIVE land mask integrated within the pycorr_iceflow workflow and a minimum correlation threshold (corr ≥0.20), the standard deviation of velocity over stable land pixels was calculated for each image pair as a measure of feature-tracking noise. Where multiple pairs were grouped into a single historical period, uncertainty is reported as the mean stable-land standard deviation across the contributing pairs.

Table 2. Landsat imagery used for glacier velocity calculations between 1985 and 1998.

Period	Satellite	Resolution (m)	Path	Row	Image date 1	Image date 2
1985-1986	Landsat 5 TM	30	017	013	27 July 1985	30 July 1986
1987-1989	Landsat 5 TM	30	018	013	24 July 1987	14 August 1989
1989-1990	Landsat 5 TM	30	018	013	14 August 1989	17 August 1990
1990-1991	Landsat 5 TM	30	018	013	17 August 1990	4 August 1991
1994-1995	Landsat 5 TM	30	018	013	11 July 1994	15 August 1995
1997-1998	Landsat 5 TM	30	018	013	19 July 1997	22 July 1998

2.3.2.3 NASA ITS_LIVE Yearly and Monthly Velocities

Surface ice velocities between 2000 and 2024 for Illaulittuuq and Maattatujana glaciers were derived from the ITS_LIVE dataset, which provides velocities estimated from optical satellite image pairs using the Hybrid Pluggable Processing Pipeline (HyP3) autoRIFT (Autonomous Repeat Image Feature Tracking) feature-tracking algorithm (Gardner and others, 2025). Velocity measurements were obtained from ITS_LIVE scene-pair products with mid-dates centred on the studied periods, primarily derived from Landsat and Sentinel-2 imagery, with a spatial resolution of 120 m.

For each glacier, the same central flowline as used for the Pycorr-derived velocities was manually digitized in the ITS_LIVE web interface (Fig. 2), exported, projected to UTM (EPSG:32620), and resampled at 120 m intervals to extract along-flow velocity time series. This resampling defines the spacing of extracted values, but does not modify the native resolution of the velocity products.

Annual and seasonal velocity series were constructed by grouping individual scene-pair measurements by year or by seasons (Winter: December-February, Spring: March-May, Summer: June-August, and Fall: September-November). For each year and season, median velocities were computed along the glacier centerlines to reduce the influence of outliers. Linear velocity trends (2000-2024) were then estimated independently at each centerline position using ordinary least-squares regression. Along-centerline trend profiles were additionally smoothed using a 1-km moving window to reduce local noise and highlight spatially coherent acceleration and deceleration patterns along the glacier flowline. Reported uncertainties are directly derived from the velocity magnitude uncertainty (v_error) provided by ITS_LIVE.

2.3.2.4 Velocity Raster Processing

Velocity fields covering the full surfaces of Illaulittuuq and Maattatujana glaciers were generated for selected image pairs from both the Pycorr and ITS_LIVE datasets. Both products provide surface velocity as horizontal components (vx, vy), from which flow direction and magnitude can be derived. The ITS_LIVE v2.1 annual mosaics provide velocity magnitude directly, while for Pycorr it was calculated as $v = \sqrt{(vx^2 + vy^2)}$. The velocity components were used to compute flow direction at each pixel, which was then compared to the circular mean direction within a 5×5-pixel neighbourhood. Vectors deviating by more than 45° from the local neighbourhood direction, or exceeding an upper velocity threshold that was unrealistically high (>200 m a^{-1}) compared to neighbouring cells, were removed as erroneous.

Following common practices used in other studies (e.g., Van Wychen and others, 2015; Schaffer and others, 2017), the remaining vectors were visually inspected and further removed where: (1) motion direction was inconsistent with observable surface flow features such as medial moraines, (2) direction changed abruptly (>45°) over short distances, or (3) velocities were anomalously high near glacier margins relative to the centerline.

The retained vectors were then rasterized to a 120 m grid to match the standard ITS_LIVE resolution. To reduce noise from individual image pairs or annual mosaics, velocity rasters were combined using the median velocity magnitude for each measurement period when multiple datasets were available, specifically the two Pycorr image pairs (1989-1990 and 1990-1991) for the historical epoch and paired annual ITS_LIVE mosaics for the modern epoch (2000-2001, 2013-2014, and 2023-2024). Remaining gaps within the manually modified RGI v7.0 glacier outlines were filled using inverse distance weighting interpolation, where gap pixels are estimated as a weighted average of surrounding valid observations, with greater weight given to closer pixels.

2.3.2.5 Field Measurements

Surface velocities on Illaulittuuq Glacier were derived from in situ GNSS measurements acquired between summer 2024 and 2025. These measurements were used to validate ITS_LIVE satellite-derived velocity estimates for the corresponding August-December 2024 period. Two

Cryologger Glacier Velocity Tracker (GVT) stations equipped with u-blox ZED-F9P multi-frequency GNSS receivers were deployed on the glacier, each recording positions for three hours per day, starting at 1200 local time (1700 UTC). Illaulittuuq Middle (67.126°N, 65.004°W) and Illaulittuuq Lower (67.172°N, 64.893°W) stations were installed in August 2024 (Figs. 2 and 3).

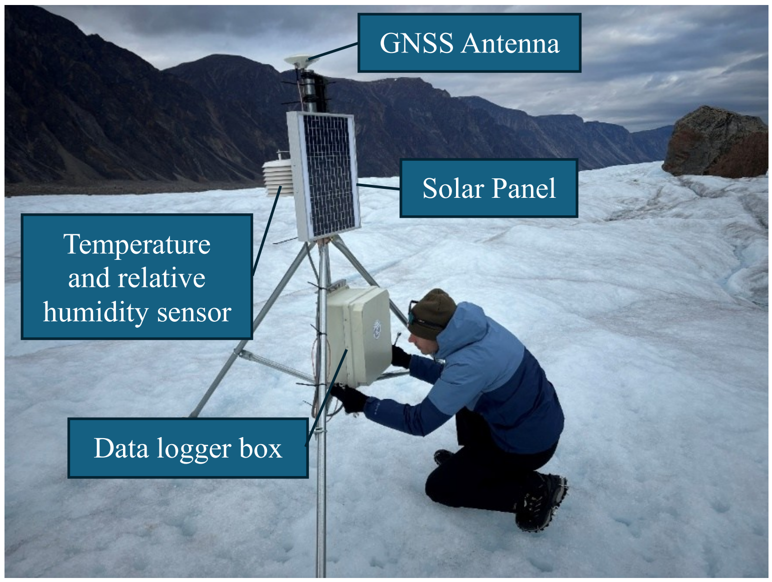

Figure 3. Illaulittuuq Glacier GVT middle station with key components in August 2024.

Raw GNSS data recorded by the Cryologger GVTs were converted from UBX (a proprietary binary format output by u-blox GNSS receivers) to daily RINEX (Receiver Independent Exchange Format) observation files, the standard format for GNSS data exchange. They were then processed using NRCan's Canadian Spatial Reference System Precise Point Positioning (CSRS-PPP) (https://webapp.csrs-scrs.nrcan-rncan.gc.ca/geod/tools-outils/ppp.php) service in kinematic mode, referenced to NAD83 (epoch 2010-01-01) with heights in CGVD2013. PPP results were extracted and concatenated across the deployment period, then summarized to daily median positions in UTM coordinates. Daily horizontal displacement was computed as the Euclidean distance between consecutive daily medians and converted to daily motion (m d^{-1}), with velocities also reported in m a^{-1}. To reduce day-to-day noise, a 5-day rolling median velocity was calculated, which facilitated the interpretation of seasonal trends.

2.3.3 Glacier Elevation

As with our velocity centerline, all elevation change rates were calculated below the equilibrium line altitude (ELA), as optical elevation data exhibit higher reliability in snow-free areas compared to snow-covered accumulation zones, where poor surface contrast and radiometric homogeneity reduce the accuracy of photogrammetric and stereo-matching techniques. The mass balance estimates presented here are not derived from the full glacier area below the ELA, but rather from a delineated zone within the ablation area where data coverage was most consistent across all study periods from 2000-2024 (Fig. 18).

2.3.3.1 1974 Historical Air Photo DEM

A 1974 DEM of Illaulittuuq Glacier was constructed from five aerial photographs (A30968_070-074, acquired on 28 July 1974) from the National Air Photo Library, Ottawa, Canada, processed using Agisoft Metashape Professional (v2.0). Camera calibration reports and six GCPs identified on stable, non-glaciated bedrock were used for camera alignment as well as sparse and dense point cloud generation. GCP coordinates were extracted from the ArcticDEM mosaic (v4.1, 2 m) in ArcGIS Pro and manually marked in each applicable image, with a mean GCP error of 3.82 m reported by Agisoft Metashape.

2.3.3.2 2000-2019 Theia Elevation Change Dataset

Glacier surface elevation change rates for the period 2000-2019 were obtained from the global DEM-differencing dataset of Hugonnet and others (2021), distributed via the Theia Land Data Centre (http://maps.theia-land.fr/couches-cartographiques-theia.html?year=2024&month=05&collection=glaciers). The dataset provides glacier surface elevation change at 100 m spatial resolution for successive 5-year periods and is derived from time-series analysis of optical stereo DEMs. Glacier outlines are based on the Randolph Glacier Inventory v7.0 (https://www.glims.org/RGI/; (RGI 7.0 Consortium, 2023). In the Canadian Arctic, elevation observations primarily originate from ASTER stereo imagery and ArcticDEM products derived from WorldView (WV) and GeoEye stereo imagery (Hugonnet and others, 2021). All DEMs were co-registered to the TanDEM-X 90 m global DEM using elevation differences over stable, ice-free terrain and subsequently bias-corrected to remove residual vertical and along-track errors, and DEMs with large residual errors were excluded. Elevation observations were filtered using spatial constraints relative to local TanDEM-X topography and temporal constraints based on physically plausible glacier elevation change rates to remove outliers and unrealistic elevation changes, with measurement uncertainty empirically characterized as a function of terrain slope, stereo-correlation quality, and DEM-specific co-registration performance (Hugonnet and others, 2021). Continuous elevation time series were then reconstructed independently for each pixel using Gaussian Process regression, allowing for irregular temporal sampling while accounting for long-term trends, seasonal variability, and short-term temporal correlation. Elevation change rates, were derived from these modelled time series and aggregated over 5-year periods to produce spatially consistent glacier surface elevation change fields across the Canadian Arctic.

2.3.3.3 2020-2024 ArcticDEM Coregistration and Differencing

To extend elevation-change estimates up to 2024, glacier surface elevations for 2020 and 2024 were derived using 2-m resolution ArcticDEM strip DEMs (https://www.pgc.umn.edu/data/arcticdem/; (Porter and others, 2022). ArcticDEM strip DEMs are derived from ~0.5 m stereo imagery acquired primarily by the WorldView satellite constellation (WV01, WV02, WV03). Elevations are extracted using the SETSM (Surface Extraction with TIN-based Search-space Minimization) stereo-photogrammetric workflow (Noh and Howat, 2015), which applies automated stereo-correlation to overlapping image pairs. Each stereo pair is first processed into smaller scene-level DEM segments, which are then co-registered and merged to generate the final strip DEM.

For both Illaulittuuq and Maattatujana glaciers in 2020, three summer strips were used (2020-07-16 WV01, 2020-07-16 WV02, and 2020-08-15 WV01). For 2024, due to limited cloud-free summer coverage, two spring acquisitions (2024-03-08 WV02 and 2024-04-17 WV01) were used for both glaciers, with an additional late-summer strip (2024-09-04 WV01) available for Illaulittuuq Glacier. Each ArcticDEM strip corresponds to a single stereo acquisition and was processed independently before mosaicking them together.

ArcticDEM strip DEMs contain systematic horizontal and vertical offsets arising from the independent georeferencing of each stereo pair, necessitating co-registration prior to differencing to ensure detected elevation changes reflect true surface change rather than geometric artefacts (Dai and Howat, 2017; Małecki, 2022). Therefore, ArcticDEM processing was performed using the pybob DEM co-registration Python package (https://github.com/iamdonovan/pybob/tree/master), which implements the algorithm of Nuth and

Kääb (2011) to estimate and correct horizontal and vertical biases by minimizing elevation differences over stable terrain. Glacierized areas were excluded using the Randolph Glacier Inventory 7.0 outline (RGI 7.0 Consortium, 2023), such that only non-glacierized terrain contributed to the estimation of co-registration parameters. Prior to co-registration, conservative filtering was applied to reduce outliers, including a ±150 m elevation-difference threshold relative to the reference DEM and a slope ≤30° land mask derived from the reference DEM to restrict stable terrain to low-slope surfaces.

To combine overlapping ArcticDEM strips within each period, while avoiding mosaicking artefacts, pixelwise median composites were generated separately for 2020 and 2024, retaining the median elevation value at each grid cell where multiple strips overlapped. Elevation change between both periods was computed by differencing the 2024 mosaicked DEM from the 2020 DEM. To remove any residual inter-period vertical bias that persisted after independent co-registration, a post-processing stable-terrain correction was applied by subtracting the median elevation difference measured over non-glacierized terrain from the full elevation-change field.

ArcticDEM-derived elevation changes for 2020-2024 were converted to annual rates to allow direct comparison across periods. Owing to variable acquisition dates among ArcticDEM strips within each mosaic, a pixelwise temporal normalization was applied: for each pixel, the exact time separation between the contributing 2020 and 2024 source acquisitions was calculated using strip acquisition dates, and elevation change was divided by this pixel-specific time interval to derive annual elevation change. Finally, to ensure consistency with the Theia dataset, ArcticDEM-derived elevation-change rates were resampled to a common 100 m grid.

For all elevation change products, uncertainty was estimated as the standard deviation of bias-corrected elevation change rate over stable, non-glacierized terrain (slopes ≤30°; Table 3), relative to the ArcticDEM mosaic (v4.1), following approaches applied in comparable glacier DEM studies (Lauzon and others, 2023; Partington and others, 2025).

Table 3. Elevation-change rate uncertainty (standard deviation)

Period	Illaulittuuq (m a^{-1})	Maattatujana (m a^{-1})
1974-2000*	0.472	-
2000-2004**	0.120	0.120
2005-2009**	0.129	0.129
2010-2014**	0.125	0.125
2015-2019**	0.144	0.144
2020-2024***	0.217	0.214

* Agisoft Metashape DEM + Theia/Hugonnet and others (2021) data
** Theia/Hugonnet and others (2021) data
*** ArcticDEM data

2.3.3.4 1974-2000 Elevation Change Rate

To estimate the glacier surface elevation change rate from 1974-2000, a 2000 elevation surface was constructed by working backward from a 2020 ArcticDEM baseline, subtracting the 5-year interval elevation change rates provided by Hugonnet and others (2021) for 2000-2019. This approach was preferred over direct DEM differencing from an earlier reference surface, as the 2020 ArcticDEM provides a high-accuracy, well-georeferenced baseline from which to work backward, minimizing the propagation of errors associated with older, less precise elevation datasets. DEM differencing between the corrected 1974 DEM and the derived 2000 elevation surface then returned mean surface elevation change rates for the 1974-2000 period.

To ensure consistency across all processing, all DEMs and DEMs strips used from 1974-2024 were reprojected to World Geodetic System 84 / Universal Transverse Mercator Zone 20N (EPSG 32620), resampled to a 10 m grid, and when required, co-registered over stable terrain to a common geometric reference: the ArcticDEM mosaic (v4.1, 10 m), used solely for alignment.

2.4 Results

2.4.1 Glacier Terminus Extent Changes

Illaulittuuq and Maattatujana glaciers both retreated continuously between 1958 and 2024, although Illaulittuuq Glacier exhibited slightly greater overall mean rate of change. Total centerline retreat reached 1.54 km (23.3 m a^{-1}; 3.49 km² area loss) for Illaulittuuq Glacier and 1.14 km (17.3 m a^{-1}; 0.91 km² area loss) for Maattatujana Glacier (Figs. 4a and 5a).

At the decadal scale, both glaciers exhibit temporal variability in retreat rates, although with contrasting patterns. Illaulittuuq Glacier retreated at ~18 m a^{-1} between 1958 and 1975, slowed to a rate of ~7 m a^{-1} between 1975 and 1985, and then underwent progressively greater retreat to reach peak values of ~37 m a^{-1} between 2005 and 2015, remaining elevated at ~34 m a^{-1} through 2024 (Figs. 4b and 4c). Overall, rates prior to 1995 were comparatively low and variable. Mean retreat rates approximately doubled from 15.8 m a^{-1} (0.038 km^2 a^{-1}) during 1958-1995 to 32.9 m a^{-1} (0.073 km^2 a^{-1}) during 1995-2024, with post-1995 rates consistently exceeding those of the preceding period.

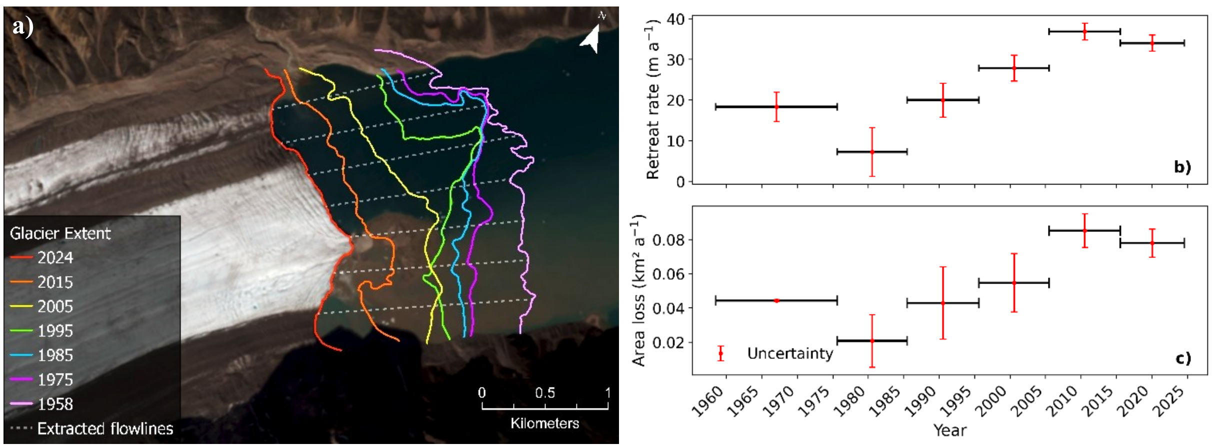

Figure 4. (a) Terminus change of Illaulittuuq Glacier from 1958-2024, displayed on Sentinel-2B image (19 July 2024); (b) retreat rate; (c) rate of area loss.

Maattatujana Glacier followed a somewhat similar pattern, characterized by three distinct phases (Fig. 5b and 5c). After moderate mean retreat rates of 15.6 m a^{-1} (0.013 km^2 a^{-1}) between 1958 and 1985, rates declined to 8.6 m a^{-1} (0.009 km^2 a^{-1}) between 1985 and 2005, before increasing sharply to ~30 m a^{-1} (0.022 km^2 a^{-1}) between 2005 and 2024.

Notably, the post-2005 acceleration in retreat of Maattatujana Glacier coincides with a period during which Illaulittuuq Glacier had already been retreating at elevated rates since the mid-1990s. Prior to their convergence in recent accelerated retreat, the two glaciers displayed different trends: Illaulittuuq Glacier showed a broadly progressive increase in retreat rates across the study period, whereas Maattatujana Glacier experienced a period of reduction in retreat rates between 1985 and 2005 before its subsequent recent acceleration.

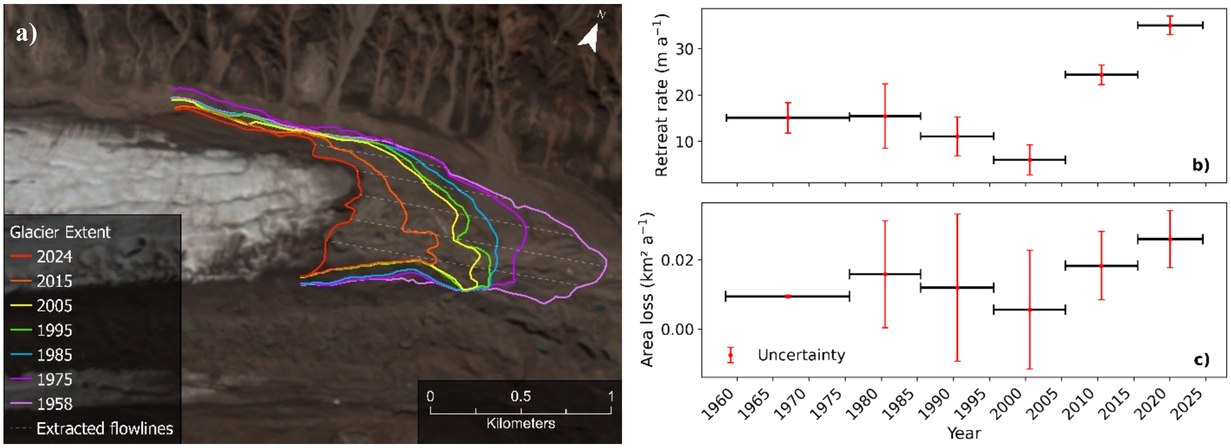

Figure 5. (a) Terminus change of Maattatujana Glacier from 1958-2024, displayed on Sentinel-2B image (19 July 2024); (b) retreat rate; (c) rate of area loss.

2.4.2 Glacier Velocity Change

2.4.2.1 Illaulittuuq Glacier velocity evolution

Annual feature tracking velocities reveal a clear down-glacier gradient at Illaulittuuq Glacier, with a mean centerline velocity of 70.4 m a^{-1} from 1985-2024. Ice flow peaks at ~180 m a^{-1} in the upper glacier, decreasing progressively toward the terminus where it reaches lows of ~12 m a^{-1} (Fig. 6). Flow speeds exceeding ~100 m a^{-1} are confined to locations above ~26.5 km from the terminus. From 1985 to 2005, mean velocities in the lower 20 km were relatively stable, ranging between 56 and 74 m a^{-1}, with a mean of 64.1 m a^{-1} (σ = 5.1 m a^{-1}). This stable trend is also evident from point velocity measurements in the lower 8 km of the terminus, which extend this trend back to 1958 (Fig. 7). From 2006-2010, a transitional period saw mean velocities in the lower 16 km decline to ~53 m a^{-1}, with increased interannual variability (range: 44-64 m a^{-1}). After 2012, velocities in the lower 16 km declined further and stabilized at ~36 m a^{-1} (σ = 3.3 m a^{-1}).

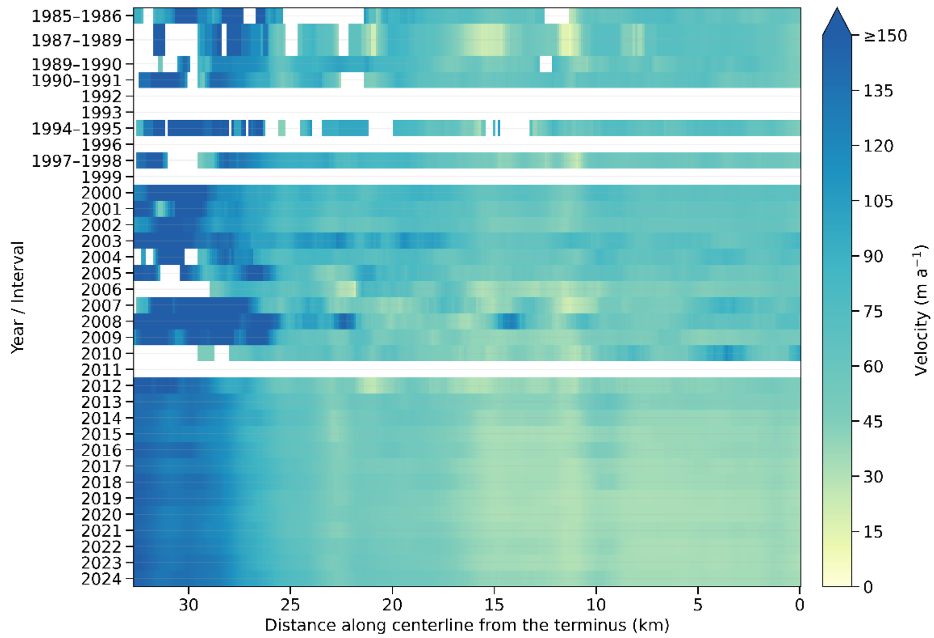

Figure 6. Pycorr (1985-1998) and ITS_LIVE (2000-2024) derived centerline velocities for Illaulittuuq Glacier with a 1 km distance smoothing. See Fig. 2 for location of centerline.

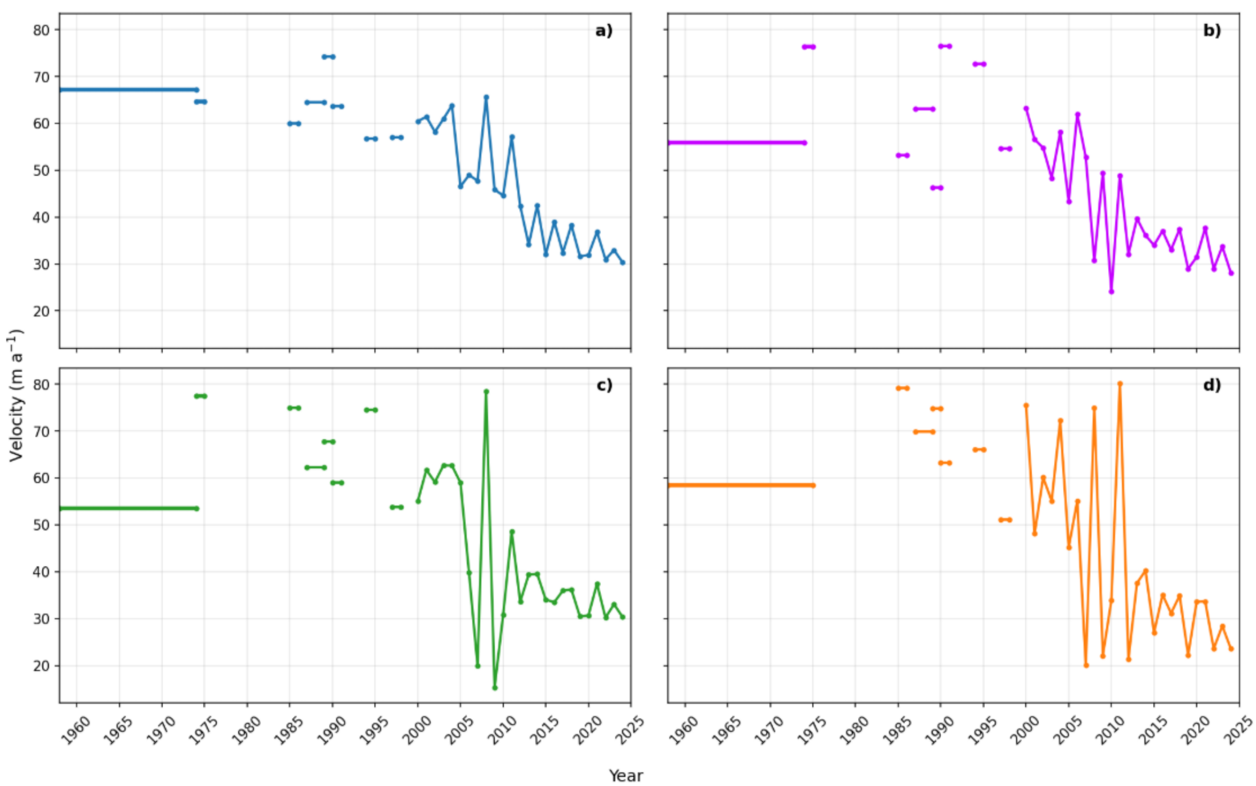

Figure 7. Point velocity measurements on the lower section of Illaulittuuq Glacier from 1958-2024 (see Fig. 2 for point locations): (a) Illaulittuuq 1: 67.188°N, 64.876°W; (b) Illaulittuuq 2: 67.172°N, 64.901°W; (c) Illaulittuuq 3: 67.169°N, 64.917°W; and (d) Illaulittuuq 4: 67.151°N, 64.945°W.

Analysis of long-term patterns over the 1985-2024 period corroborates these observations (Fig. 8), with approximately 88% of centerline measurement locations within 26.5 km of the terminus exhibiting statistically significant negative velocity trends and a mean deceleration of -0.91 m a^{-2} across that zone. This provides statistical confidence in the velocity reductions observed across the lower glacier. Above 26.5 km from the terminus, a mean deceleration of -0.65 m a^{-2} is observed, but the change is statistically significant at only 23% of measurement locations and the range spans from -1.80 to +0.92 m a^{-2}, indicating high spatial variability that warrants cautious interpretation of long-term velocity changes in the upper glacier.

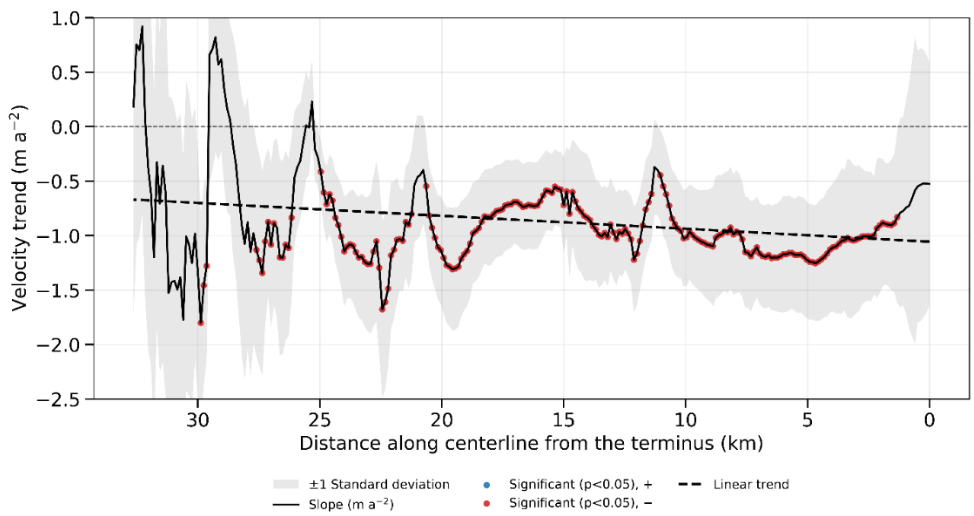

Figure 8. Centerline velocity trends for Illaulittuuq Glacier (1985-2024). Trend slopes (m a^{-2}) were estimated from linear regression with 1 km distance smoothing. Coloured points indicate statistically significant trends ($p < 0.05$): blue denotes acceleration and red denotes deceleration. Distance is measured from the terminus. See Fig. 2 for location of centerline.

Velocity distribution maps provide further insight into the spatial distribution of velocity changes across Illaulittuuq Glacier (Fig. 9). In the late 1980s to early 2000s, moderate to high velocities were broadly distributed across the glacier (Fig. 9a, b), consistent with the relatively stable flow conditions identified in the centerline record during that period. By the 2010s and early 2020s, velocity reductions are most pronounced along the main trunk, where the strongest deceleration progressively dominates toward the terminus, while the northern tributary exhibits a less intense deceleration (Fig. 9c, d). Velocity vectors align well with valley geometry and surface features such as medial moraines, providing confidence in the spatial integrity of the velocity products.

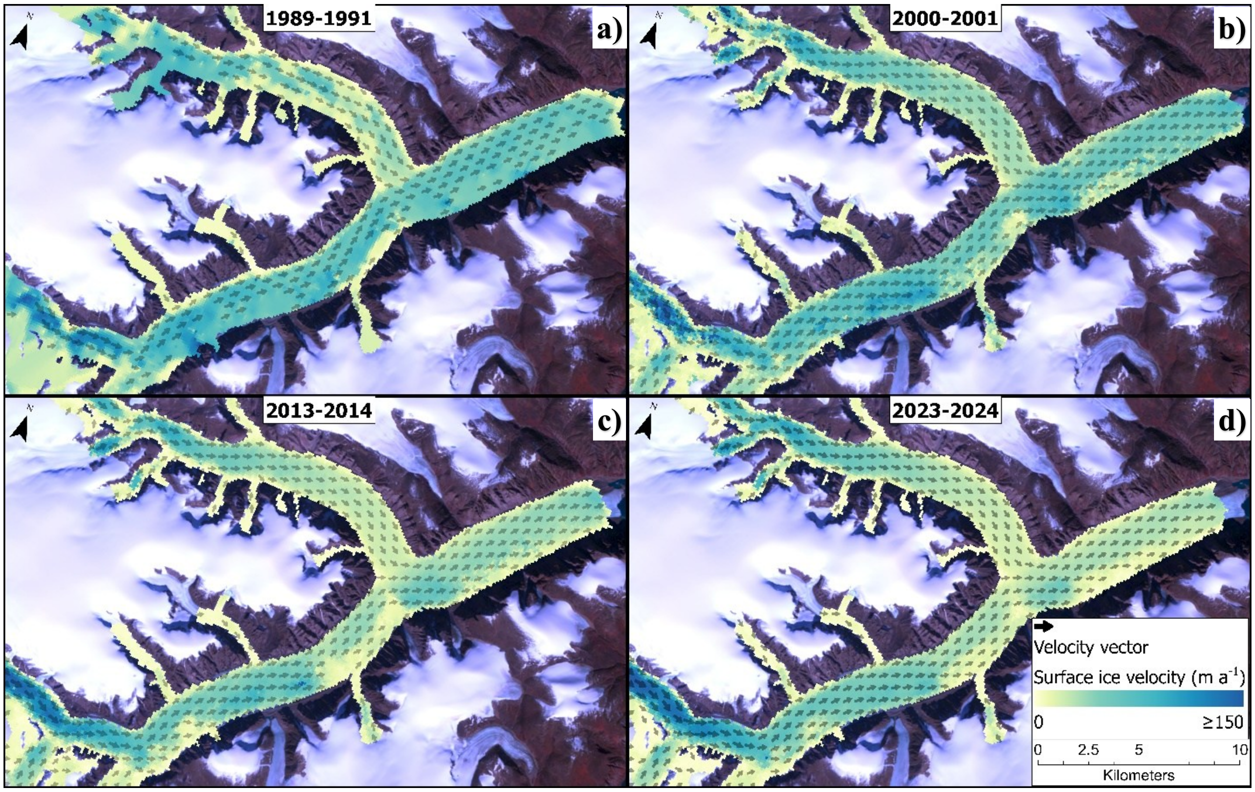

Figure 9. Spatial distribution of surface ice velocity at Illaulittuuq Glacier for four representative periods: (a) 1989-1991; (b) 2000-2001; (c) 2013-2014; (d) 2023-2024. Colours show surface velocity magnitude (m a^{-1}) and arrows indicate flow direction and relative magnitude. Base map from Landsat 5, 16 September 2020.

2.4.2.2 Maattatujana Glacier velocity evolution

Maattatujana Glacier is a comparatively slower flowing system than Illaulittuuq Glacier, with a mean centerline velocity of 59.0 m a^{-1} from 1985-2024, and a down-glacier velocity gradient that transitions from ~180 m a^{-1} in the upper glacier to lows of ~10 m a^{-1} near the terminus (Fig. 10). From 1985 to 2006 in the lower 15 km, and since 1958 at least in the lower 4 km (Fig. 11), flow conditions were stable, with mean velocities of 50.1 m a^{-1} (σ = 3.0 m a^{-1}; range: 44-55 m a^{-1}). Beginning around 2006, a period of progressive deceleration occurred, with mean velocities declining to 37.9 m a^{-1} (σ = 7.1 m a^{-1}; range: 29-49 m a^{-1}) through 2013. Thereafter, velocities stabilized at 27.5 m a^{-1} (σ = 3.0 m a^{-1}), representing a ~45% reduction relative to the 1985-2006 mean.

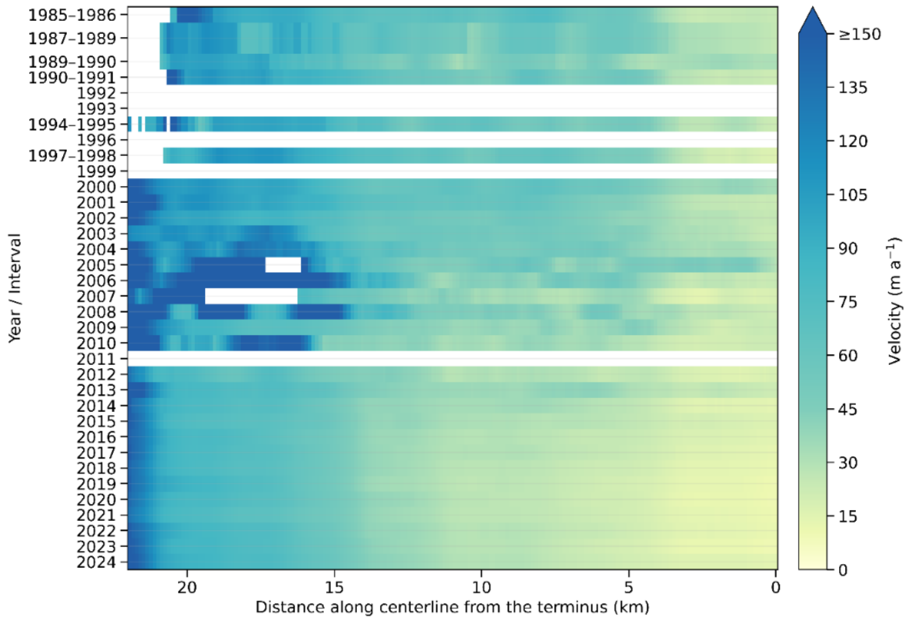

Figure 10. Pycorr (1985-1998) and ITS_LIVE (2000-2024) derived centerline velocities for Maattatujana Glacier with a 1 km distance smoothing. See Fig. 2 for location of centerline

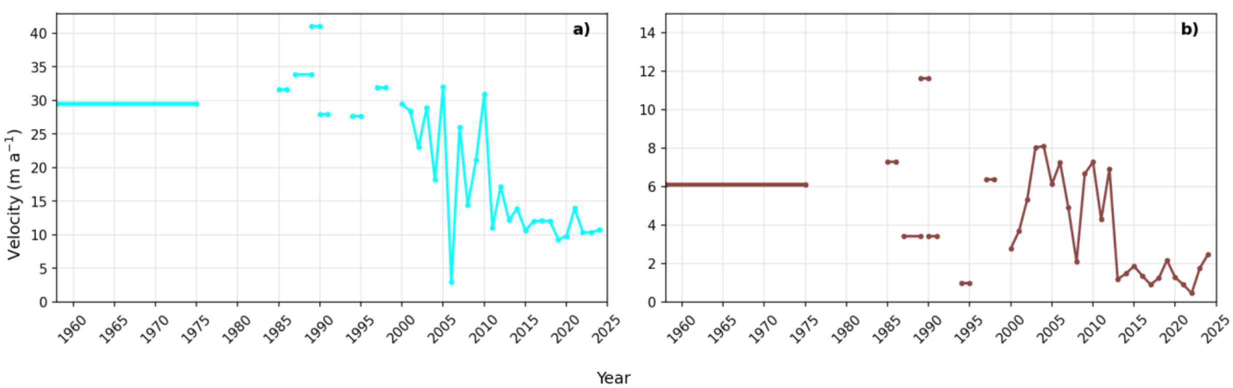

Figure 11. Point velocity measurements on the lower section of Maattatujana Glacier from 1958-2024 (see Fig. 2 for point locations): (a) Maattatujana 1: 67.360°N, 65.200°W; (b) Maattatujana 2: 67.368°N, 65.158°W. Note different scales between figure parts.

Analysis of changes over the study period indicates negative velocity trends across the entire Maattatujana Glacier centerline, with statistically consistent deceleration confined to locations below 15 km (Fig. 12). Within this zone, the strongest deceleration occurs between 5 and 15 km from the terminus, where 100% of measurement locations show significant negative trends with a mean rate of -1.02 m a^{-2}, while the 0-5 km zone shows a comparatively weaker but equally consistent signal at -0.60 m a^{-2}. Above 15 km from the terminus, despite uniformly negative trends, minimal statistical significance is present, reflecting high spatial variability that warrants cautious interpretation of changes over the upper glacier.

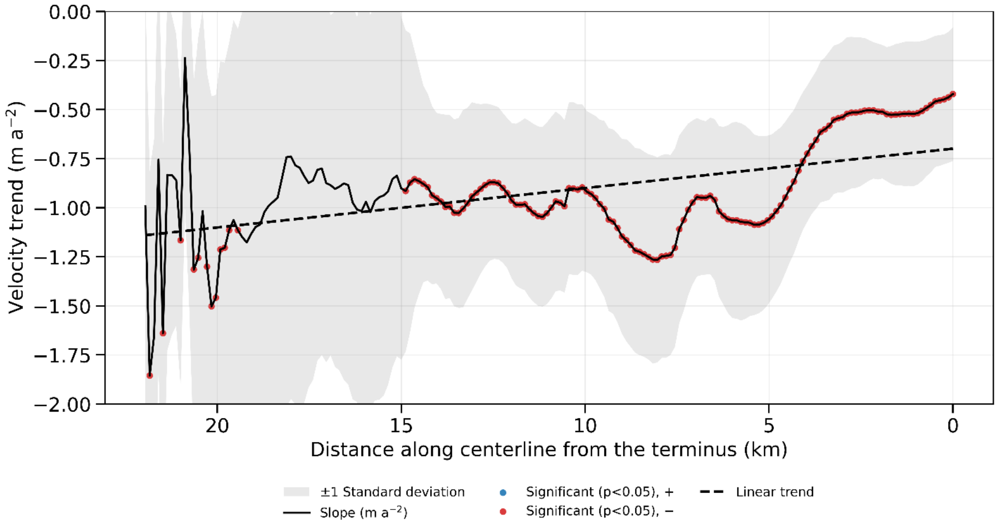

Figure 12. Centerline velocity trends for Maattatujana Glacier (1985-2024). Trend slopes (m a^{-2}) were estimated from linear regression with 1 km distance smoothing. Coloured points indicate statistically significant trends ($p < 0.05$): blue denotes acceleration and red denotes deceleration. Distance is measured from the terminus. See Fig. 2 for location of centerline.

Glacier-wide velocity fields of Maattatujana Glacier show moderate velocities across most of the main trunk and both southern tributaries in the 1989-1991 and 2000-2001 periods (Fig. 13a, b). By 2013-2014, both southern tributaries show marked velocity reductions (Fig. 13c), becoming more pronounced through 2023-2024 (Fig. 13d), suggesting a progressive decrease in their contribution to overall glacier flow. Velocity vectors align well with glacier flow structure and valley geometry, providing confidence in the spatial representativeness of the velocity products.

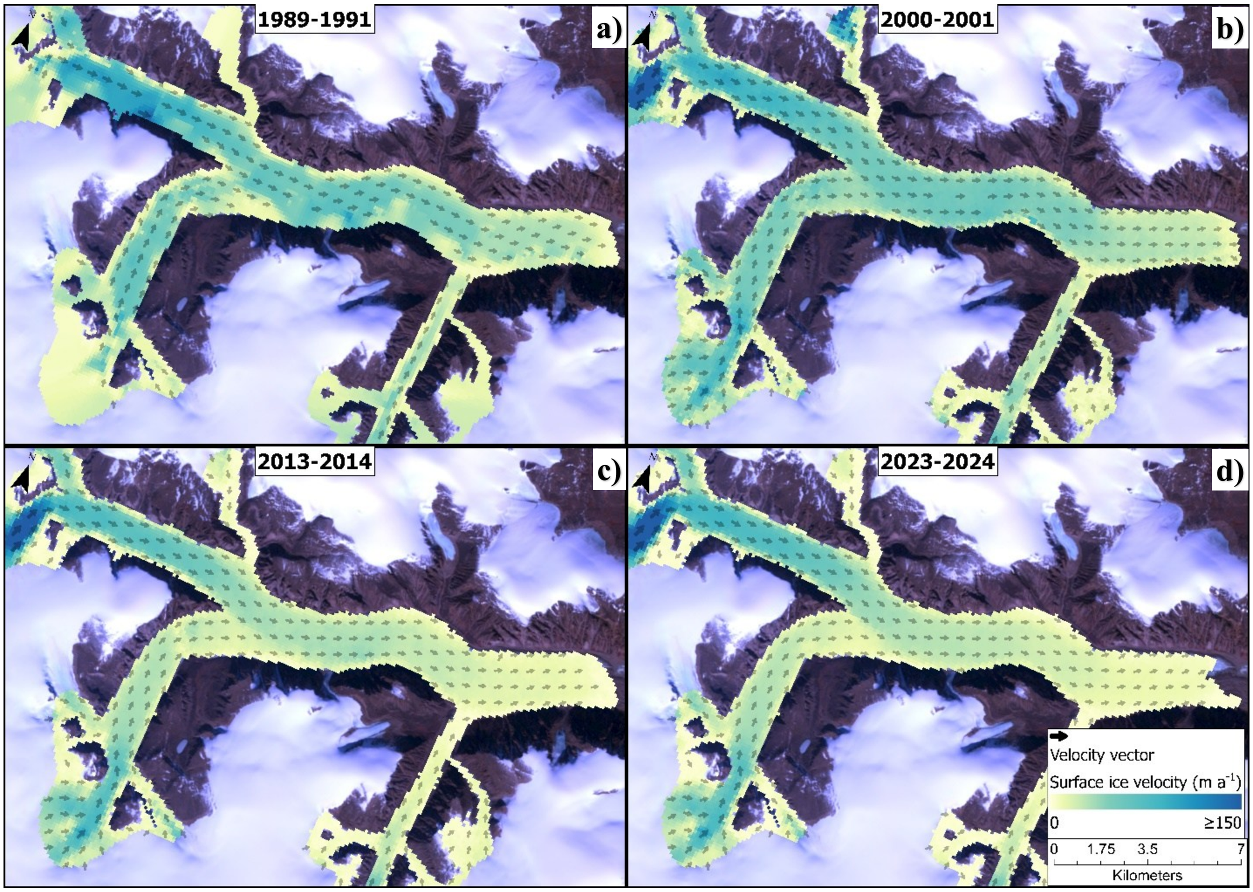

Figure 13. Spatial distribution of surface ice velocity at Maattatujana Glacier for four representative periods: (a) 1989-1991; (b) 2000-2001; (c) 2013-2014; (d) 2023-2024. Colours show surface velocity magnitude (m a^{-1}) and arrows indicate flow direction and relative magnitude. Base map from Landsat 5, 16 September 2020.

2.4.2.3 Seasonal velocity variability and trends

GNSS velocity records from the two on-ice stations at approximately 4 km and 11 km from the terminus of Illaulittuuq Glacier were examined using the standard four three-month seasons for the region, winter (DJF), spring (MAM), summer (JJA), and fall (SON), consistent with the seasonal framework used in the subsequent ITS_LIVE seasonal trend analysis. While transitions between seasons are gradual rather than sharply defined, velocities at both stations show characteristic patterns within each period (Fig. 14a, b). During winter, velocities at both stations are low and stable, with minimal day-to-day variability. Spring shows an early melt season signal with modest velocity increases and episodic short-duration peaks, particularly at the middle station, while summer is characterized by the highest and most variable velocities, including pronounced speed-up events likely driven by peak surface melt and subglacial water pressure pulses. Fall marks a transitional period of declining and increasingly stable velocities returning toward winter baseline conditions.

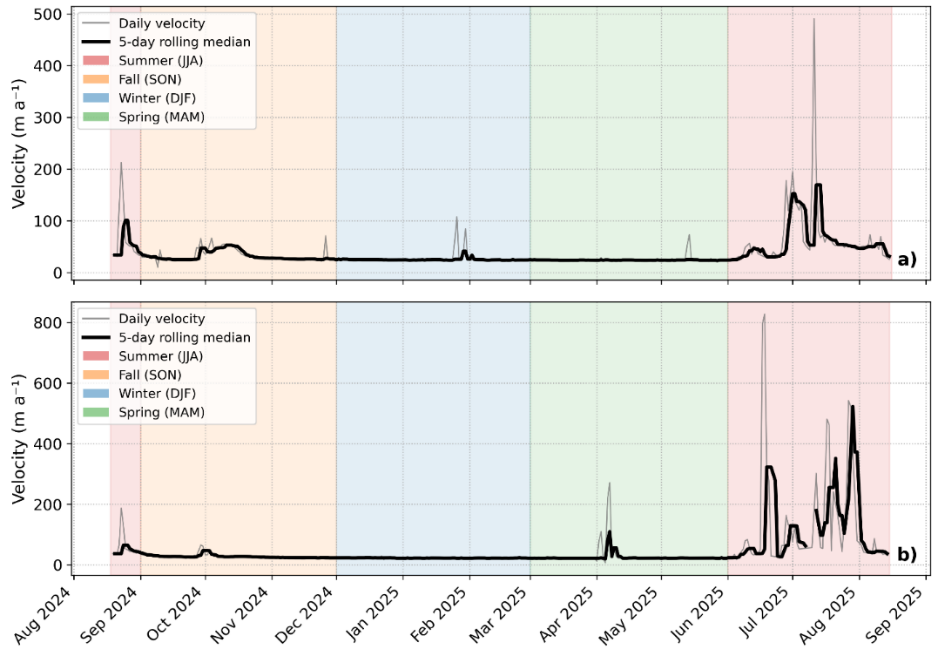

Figure 14. GNSS-derived ice surface velocity records at two GVT stations on Illaulittuuq Glacier: (a) Middle (67.1258° N, 65.0040° W); (b) Lower (67.1727° N, 64.8933° W). Velocity records span August 2024 to August 2025, with the solid black line showing 5-day rolling medians. Seasonal periods are indicated by background shading. See Fig. 2 for location of stations.

Analysis of ITS_LIVE velocities from 2000 to 2024 indicates that long-term deceleration is expressed across all seasons at both glaciers, but with pronounced differences in magnitude between seasons. At Illaulittuuq Glacier, spring and summer show the strongest deceleration within the lower 26.5 km, with mean trends of -2.79 m a^{-2} and -2.72 m a^{-2}, respectively, and statistical significance at >88% of measurement locations in both seasons (Fig. 15a-d). Winter and fall show comparatively weaker, but still predominantly negative trends, with mean deceleration rates of -0.98 m a^{-2} and -0.86 m a^{-2}, and significance of 85.5% and 68.8%, respectively.

Maattatujana Glacier shows a similar seasonal structure, but with a more pronounced contrast between seasons (Fig. 15e-h). Spring deceleration dominates at -3.77 m a^{-2}, with 100% of measurement locations significant within the lower 15 km, followed by summer at -2.21 m a^{-2}. Winter and fall show weaker deceleration of -0.88 and -1.02 m a^{-2}, respectively, with fall showing the lowest statistical confidence at both glaciers. Overall, while long-term deceleration has occurred across all seasons, it is most pronounced during spring and summer at both glaciers.

Independent validation with GNSS position measurements recorded at the Illaulittuuq Glacier GVT stations during August-December 2024 shows good agreement with ITS_LIVE satellite velocities. At Illaulittuuq Middle Station, ITS_LIVE measured 33.0 m a^{-1} compared to 26.7 m a^{-1} from our GVT, and at Illaulittuuq Lower Station, ITS_LIVE measured 32.0 m a^{-1} compared to 25.5 m a^{-1}. This agreement between field and satellite measurements supports the reliability of the ITS_LIVE velocities used in our analyses on a seasonal scale.

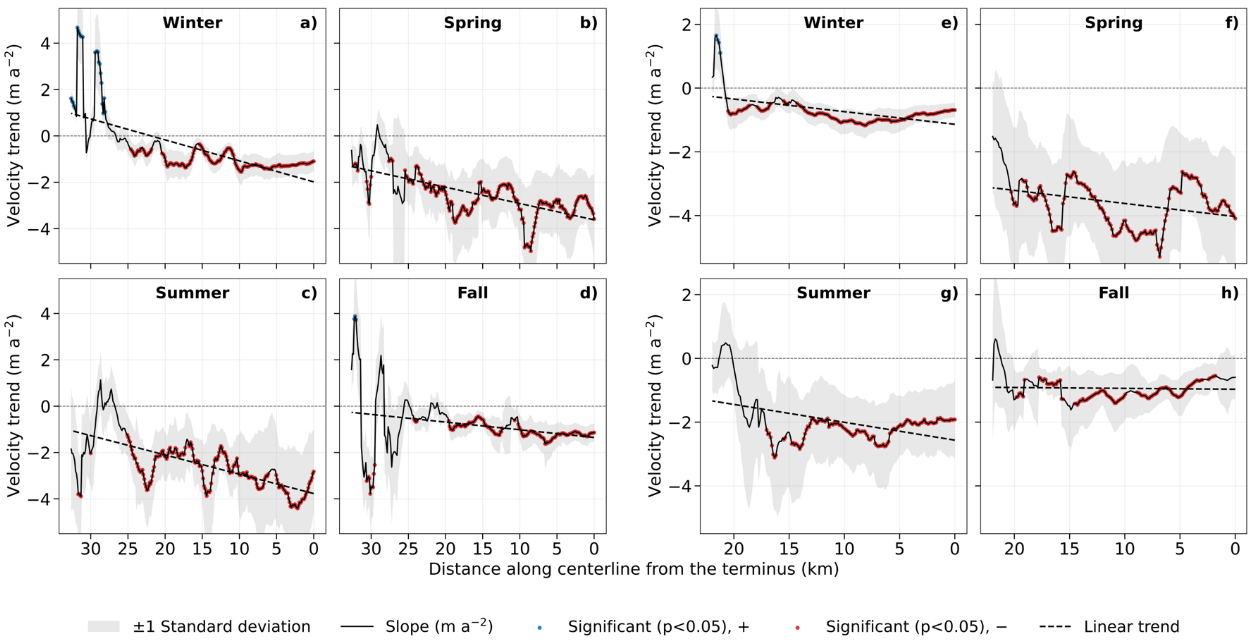

Figure 15. (a-d) Illaulittuuq Glacier and (e-h) Maattatujana Glacier seasonal centerline velocity trends (2000-2024) for winter (DJF), spring (MAM), summer (JJA), and fall (SON), respectively. Trend slopes (m a^{-2}) were estimated via linear regression applied to seasonal ITS_LIVE velocity medians with 1 km distance smoothing. Coloured points indicate statistically significant trends ($p < 0.05$): blue indicates acceleration and red indicates deceleration.

2.4.3 Surface Elevation Change

Overall, the centerline of Illaulittuuq Glacier experienced surface lowering between 2000 and 2024, with the strongest thinning concentrated in the lower section of the glacier (Fig. 16). From 2000-2004, median centerline elevation change rates were near zero (-0.25 m a^{-1}), indicating approximate stability during this earliest period. Thinning accelerated substantially in subsequent periods, with median centerline rates reaching -0.72 m a^{-1} from 2005-2009, -1.87 m a^{-1} from 2010-2014, and peaking at -2.21 m a^{-1} from 2015-2019. The 2020-2024 period shows a partial reduction in thinning rates to a median of -1.06 m a^{-1}, although this period relies on a different DEM source than preceding periods and should be compared with caution.

Spatially, thinning is most pronounced in the lower 12.5 km (Table 4). Within approximately 5 km of the terminus, mean elevation change rates remain relatively stable below about -1.5 m a^{-1} prior to a marked acceleration after 2009, when rates reached up to about -3 m a^{-1}. Across the full lower 12.5 km, median elevation change rates progressed from near-zero from 2000-2004 to -3.33 m a^{-1} from 2015-2019, before partially reducing to -1.90 m a^{-1} from 2020-2024. The 12.5-25 km zone shows a similar but less intense intensification pattern but still seeing four to five-fold increases in median elevation change rates since 2004. Above 25 km, median values remain close to zero throughout all periods.

Table 4. Illaulittuuq Glacier median centerline elevation change rate (m a^{-1}) per 5-year periods across varying glacier zones (distances are from the terminus).

Period	0-5 km	0-12.5 km	12.5-25 km	25-32.2 km
1974-2000	-0.91	-	-	-
2000-2004	-0.60	0.11	-0.34	-0.41
2005-2009	-1.54	-1.07	-0.80	-0.29
2010-2014	-2.40	-2.89	-1.65	0.06
2015-2019	-2.99	-3.35	-2.03	0.09
2020-2024	-2.05	-1.88	-1.74	-0.16

Maattatujana Glacier shows a contrasting pattern, characterized by comparatively uniform thinning rates across all periods, with overall median centerline rates ranging narrowly between -1.22 and 1.59 m a^{-1} throughout the study period (Fig. 17). This sustained and relatively stable thinning signal contrasts with the pronounced temporal variability observed at Illaulittuuq Glacier. Spatially, it is notable that Maattatujana's lower 5 km shows progressive intensification in thinning, with median elevation change rates more than doubling since the 2000-2004 period, increasing to the point of surpassing rates of -2 m a^{-1} (Table 5). In contrast, the zone above 5 km shows a reversed temporal evolution, with median thinning rates declining over time from -1.33 to -0.71 m a^{-1} from 2000-2004 to 2020-2024.

Table 5. Maattatujana Glacier median centerline elevation change rate (m a^{-1}) per 5-year periods across varying glacier zones (distances are from the terminus).

Period	0-5 km	>5 km
2000-2004	-0.87	-1.33
2005-2009	-1.74	-1.28
2010-2014	-1.84	-1.16
2015-2019	-2.44	-0.02
2020-2024	-2.11	-0.71

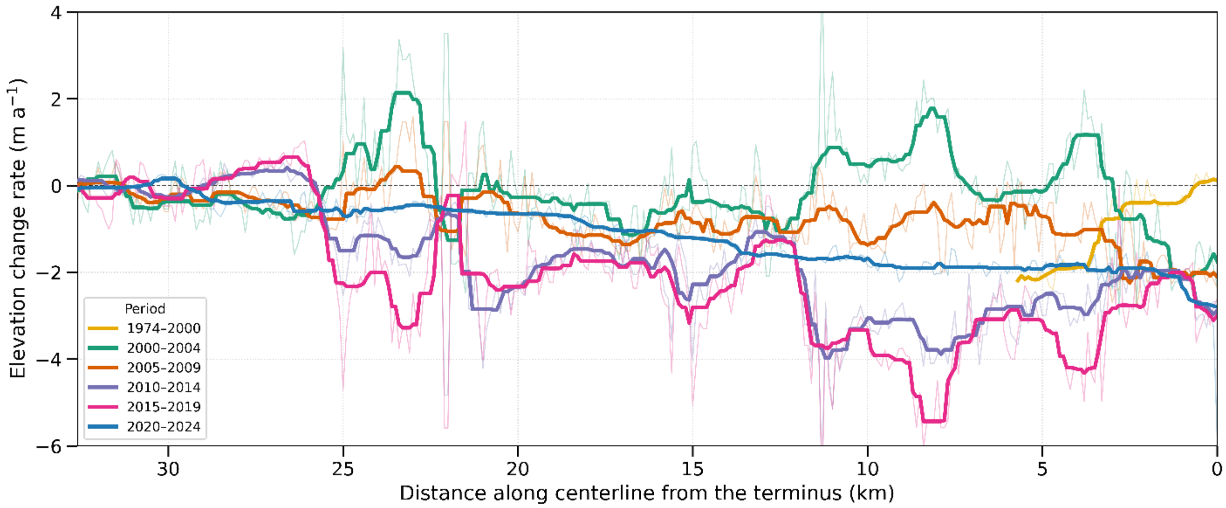

Figure 16. Centerline elevation change rates along Illaulittuuq Glacier centerline from 2000-2024. Faded lines show raw sampled values and solid lines show 1 km rolling median profiles. Elevation change rates for 2000-2019 are derived from Hugonnet and others (2021), while the 2020-2024 period is derived from ArcticDEM strips. Historical DEM derived elevation change rate from 1974-2000 is presented only for the terminus section. See Fig. 2 for location of centerline.

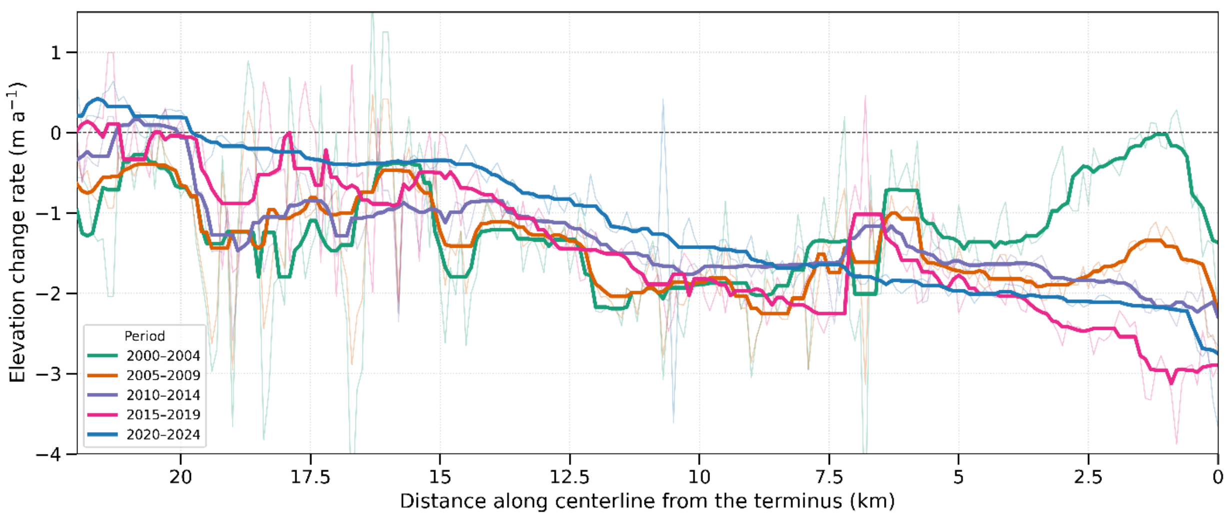

Figure 17. Centerline elevation change rates along Maattatujana Glacier centerline from 2000-2024. Faded lines show raw sampled values and solid lines show 1 km rolling median profiles. Elevation change rates for 2000-2019 are derived from Hugonnet and others (2021), while the 2020-2024 period is derived from ArcticDEM strips. See Fig. 2 for location of centerline.

2.5 Discussion

2.5.1 Decoupling of Illaulittuuq Glacier's Dynamics from Marine Terminus Influence

When examining the changes of marine-terminating Illaulittuuq Glacier, the velocity structure is inconsistent with patterns typically associated with an active marine-terminating glacier system. From 1985 to 2024, surface velocities peak at approximately 180 m a^{-1} in the upper glacier and decline progressively toward the calving front, reaching approximately 12 m a^{-1} near the terminus (Figs. 6, 9). In contrast, active marine-terminating glaciers tend to display sustained or increased velocities toward their calving margins, such as those in the northern CAA which often reach 300 m a^{-1} (Van Wychen and others, 2014), and sometimes exceed 700 m a^{-1} at highly dynamic outlets (Dalton and others, 2022). Instead, what we observe at Illaulittuuq Glacier is more consistent with that of smaller marine-terminating and land-terminating glaciers in the southern CAA that typically attain peak velocities near their equilibrium line and decelerate toward their termini (Van Wychen and others, 2015; Millan and others, 2017). Maattatujana Glacier, with no marine connection, shows a nearly identical spatial velocity structure to Illaulittuuq: upper glacier velocities of similar magnitude, declining to approximately 10 m a^{-1} near its land terminus (Figs. 10, 13).

The long-term velocity trend at both Illaulittuuq and Maattatujana glaciers reinforces the interpretation that Illaulittuuq's marine terminus has a limited impact on its dynamics. At Illaulittuuq Glacier, statistically significant deceleration is observed across 88% of the lower 26.5 km from 1985 to 2024 (Fig. 8), with no clear acceleration phase in the record (Fig. 6), a pattern that is also observed at Maattatujana Glacier (Figs. 10, 12). At a marine-terminating glacier governed by frontal dynamics, changes in terminus geometry and frontal position (Fig. 4) would be expected to drive velocity responses as the terminus location changes and reacts to varying basal conditions, calving events, and sea ice forcing (Amundson, 2016; Brinkerhoff and others, 2017; Deakin and others, 2026). However, this is not the case at Illaulittuuq Glacier, as the long-term velocity record shows only steady decline, with no acceleration signal in the ~40-year record, just as it is for Maattatujana Glacier. Having two adjacent glaciers, from the same ice cap, under the same regional climate, producing similar velocity profiles regardless of terminus type, points toward a shared glaciological control rather than one strongly controlled by marine or land influences.

Setting aside velocities, Illaulittuuq and Maattatujana glaciers exhibit similar retreat rates despite their differing marine vs. land-terminating terminus types, retreating at 23.3 m a^{-1} and 17.3 m a^{-1}, respectively, between 1958 and 2024 (Figs. 4, 5). Although Illaulittuuq Glacier has lost roughly four times the terminus area of Maattatujana Glacier, this can be largely explained by its terminus being ~1.7 times wider. There also appears to be a delayed response at Maattatujana

Glacier relative to Illaulittuuq Glacier, with enhanced retreat at Maattatujana Glacier being evident from 2005 onward, compared to 1995 onward at Illaulittuuq Glacier. Nonetheless, both glaciers show retreat rates exceeding 30 m a^{-1} within the last 20 years, suggesting that this increased terminus retreat may not be solely related to terminus type but simply a delayed response to a shared climate forcing.

2.5.2 Mass Balance of Illaulittuuq and Maattatujana Glaciers

To assess the relative importance of surface melt versus iceberg calving in accounting for the mass losses from Illaulittuuq and Maattatujana glaciers, we can use our results to compute their geodetic mass balance and dynamic discharge. Geodetic mass balance was computed by multiplying the area of the main trunk of each glacier (Fig. 18; updated with the terminus outline from the mid-date of each 5-year period between 2000 and 2024) by its thinning rate over each period. Dynamic discharge (assumed to be equivalent to iceberg calving rate) for Illaulittuuq Glacier was calculated by multiplying the surface velocity by ice thickness for a U-shaped cross-section 1 km upstream of the 2024 terminus, following the methodology of Van Wychen and others (2015). Ice thickness was derived from ArcticDEM glacier surface elevations above sea level added to a 35 m assumed ice depth below sea level (based on 2024 CTD measurements of ocean depth at the terminus), tapering to 10 m at the margins. ArcticDEM glacier surface elevations were adjusted to annual values using elevation change rates from Hugonnet et al. (2021) for 2000-2020, and differencing 2020 and 2024 ArcticDEM surfaces for 2021-2024. Annual surface velocities from 2000-2024 were obtained from the ITS_LIVE velocity mosaic. For polythermal glaciers of similar scale in the Canadian Arctic, Thomson and Copland (2017) showed that depth-averaged velocity is approximately 95% of surface velocity, so we used surface velocity directly as a proxy for depth-averaged velocity.

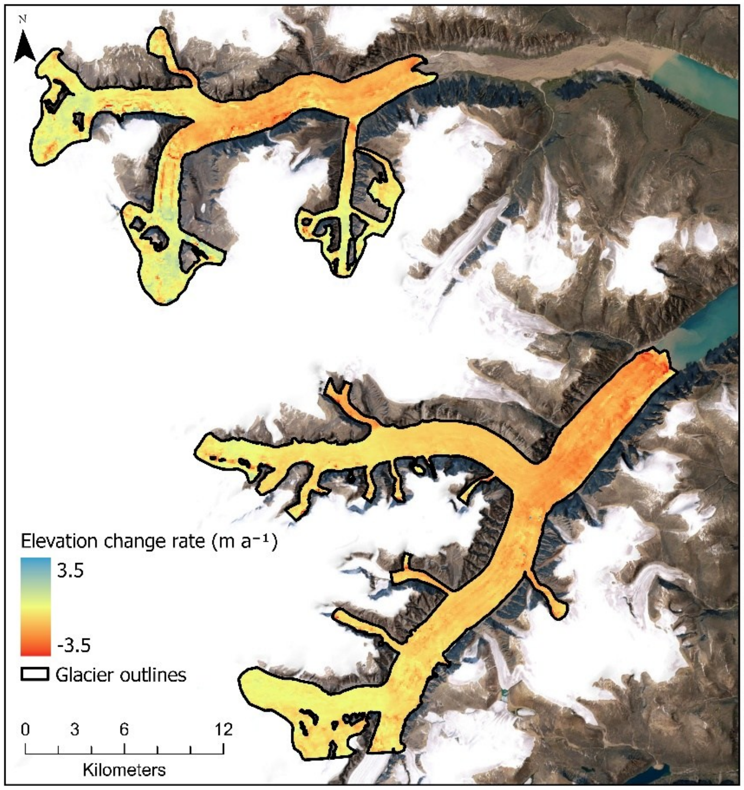

Figure 18. Mean elevation change rate for Maattatujana and Illaulittuuq glaciers from 2000-2024 superimposed on the 2002 glacier outline used for the geodetic mass balance calculations.

These calculations indicate that dynamic discharge accounted for 47.57% of total mass loss of Illaulittuuq Glacier in 2000-04 (12.63 Mt a^{-1}), then progressively declined in importance over each subsequent time period, reaching only 2.74% by 2020-24 (Fig. 19; Table 6). This decline is not simply a result of total mass loss increasing during a period of rapidly increasing geodetic mass losses, since dynamic discharge also fell in absolute terms, from 12.63 Mt a^{-1} in 2000-04 to 5.25 Mt a^{-1} in 2020-24 (Table 7). This decline in dynamic discharge reflects sustained thinning (from an ice thickness of 161.8 m to 125.2 m) and deceleration (from 54.7 to 28.3 m a^{-1}) at the flux gate over the period 2000-24, rather than any change in terminus geometry. Together, these trends indicate that dynamic discharge processes have become progressively less important to Illaulittuuq Glacier's mass budget over the study period, despite its marine terminus. This is consistent with the results from Van Wychen and others (2015), who found that dynamic discharge accounts for a considerably smaller proportion of total ablation than surface melt and runoff across the southern CAA.

In contrast, Maattatujana Glacier experienced higher mass losses in the early parts of the study period, but a more gradual decline overall, with a 27% reduction in geodetic mass balance losses from 113.80 Mt a^{-1} in 2000-04 to 82.53 Mt a^{-1} in 2020-24 (Table 6). Some of this moderation in mass losses could be attributed to accumulating debris cover that insulates the glacier surface from melt, although further investigations would be needed to confirm this.

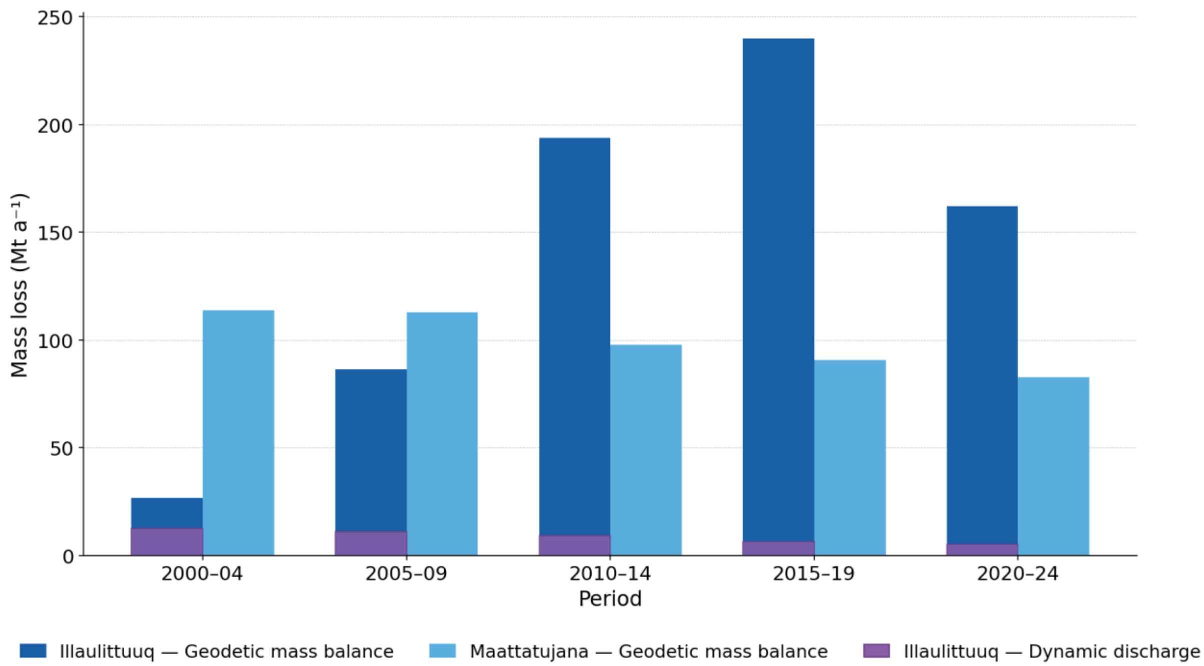

Figure 19. Mass losses from Illaulittuuq and glaciers, 2000-2024, partitioned into surface melt (derived from geodetic mass balance over the ablation area; Fig. 18) and dynamic discharge computed at a flux gate 1 km upglacier from the terminus (for Illaulittuuq Glacier).

Table 6. Ablation area and elevation change values used for calculating geodetic mass balance of Illaulittuuq and Maattatujana glaciers. Ice density assumed to be 900 kg m^{-3}.

Glacier	Period	Area (m^2)	Average elevation change (m a^{-1})	Geodetic mass balance (Mt a^{-1})
Illaulittuuq	2000-04	157,887,200	-0.19	-26.55
	2005-09	157,338,200	-0.61	-86.31
	2010-14	156,830,900	-1.37	-193.67
	2015-19	156,331,400	-1.71	-240.00
	2020-24	155,927,900	-1.15	-191.89
Maattatujana	2000-04	105,468,800	-1.20	-113.80
	2005-09	105,322,200	-1.19	-112.83
	2010-14	105,335,100	-1.03	-97.71
	2015-19	105,214,300	-0.96	-90.64
	2020-24	105,123,700	-0.87	-82.53

Table 7. Dynamic discharge for Illaulittuuq Glacier computed by integrating ice thickness with surface velocity from ITS_LIVE annual mosaics, converted to mass flux using an ice density of 900 kg m^{-3}.

Period	Mean centerline ice thickness (m)	Width (m)	Mean surface velocity (m a^{-1})	Mass discharge (Mt a^{-1})
2000-04	161.8	2,249	54.7	12.63
2005-09	157.9	2,249	50.5	11.00
2010-14	150.1	2,249	41.1	9.14
2015-19	137.7	2,249	31.7	6.37
2020-24	125.2	2,249	28.3	5.25

2.5.3. Thinning as a Driver of Velocity Decline at Illaulittuuq and Maattatujana Glaciers

The similarities between Illaulittuuq and Maattatujana glaciers presented above suggest that observed velocity changes since 2000 are primarily a response to thinning, rather than terminus type. The dependence of declining velocities on mass loss is evident in the spatial relationship between surface thinning and deceleration on both glaciers. At Illaulittuuq, surface lowering is most pronounced in the lower 12.5 km of the glacier, intensifying from near-stable conditions of +0.02 m a^{-1} in 2000-04 to a peak of -3.33 m a^{-1} from 2015-19, with a mean thinning rate of -1.81 m a^{-1} across the full 2000-2024 period (Fig. 16). This zone of maximum thinning coincides with some of the most consistent velocity declines along the glacier, where mean velocity over the lower 12.5 km declined by 47.5% between 2000-04 and 2020-24 (Fig. 6). This connection between mass losses and changes in surface velocity also extends along the full centerline of Illaulittuuq Glacier, where a mean surface thinning rate of -1.17 m a^{-1} (Fig. 16) and a mean deceleration trend of -1.37 ± 0.53 m a^{-2} are recorded over 2000 to 2024 (Fig. 8). Maattatujana Glacier shows a similar glacier-wide pattern, with a mean centerline thinning rate of -1.31 m a^{-1} (Fig. 17), and a mean deceleration trend of -1.62 ± 0.56 m a^{-2} (Fig. 12), over the same period.

This co-location of maximum thinning and elevated deceleration is consistent with progressive loss of driving stress as ice thins, reducing the gravitational force that sustains flow (Cuffey and Paterson, 2010; Ghosh et al., 2026). This mechanism has been demonstrated to be responsible for velocity reductions at other land-terminating glaciers on Penny Ice Cap (Heid and Kääb, 2012; Schaffer and others, 2017), as well as in other regions undergoing sustained negative mass balance (Thomson and Copland, 2017b; Dehecq and others, 2019; Zhou and others, 2021; Ghosh and others, 2026).

Maattatujana Glacier, having no marine connection, derives its entire mass budget from surface and internal glacier processes by definition, with no calving. Illaulittuuq Glacier is now governed by increasingly similar processes given that approximately 97% of its mass loss is attributable to surface and internal mass balance from 2020-2024, rather than dynamic discharge (Fig. 19). Together, this shift toward surface-driven mass loss and the matching deceleration trend show that Illaulittuuq's marine terminus has limited influence on the glacier's overall response to climate forcing.

Under continued warming, with future mass loss projected to concentrate at Penny Ice Cap's low-elevation margins (Schaffer and others, 2023), the declining velocities, progressive thinning, and sustained retreat documented here point toward continued reductions in ice delivery to the terminus, further diminishing Illaulittuuq Glacier's already modest and declining calving contribution, consistent with the broader pattern of limited dynamic discharge across the southern Canadian Arctic Archipelago (Van Wychen and others, 2015). Maattatujana Glacier offers a useful preview of this trajectory, showing what atmospheric-driven retreat looks like without any marine influence: glacier-wide thinning, continued terminus retreat, and deceleration as thinning reduces driving stress. Whether Illaulittuuq's terminus will eventually retreat onto land cannot be determined from the available data and would require bed topography measurements. Illaulittuuq Glacier is therefore still, technically, a calving glacier, but under sustained surface mass loss it now behaves overwhelmingly like a land-terminating glacier, with its marine terminus becoming incrementally less influential to how it behaves.

2.5.4 Flow Mechanisms under Sustained Thinning

Both Illaulittuuq and Maattatujana glaciers display a pronounced downglacier deceleration that provides insights into how flow mechanisms vary along their length. To quantify these patterns, and how they might have changed over time, ice motion due to internal deformation was estimated following methods outlined in Thomson and Copland (2017) using Glen's Flow Law, assuming an ice density of 900 kg m^{-3}. Since measurements of ice temperature are not available for either glacier, a value of -5°C was assumed, consistent with the approaches used for similar CAA outlet glaciers (Pimentel and others, 2017; Schaffer and others, 2017; Thomson and Copland, 2017b). A shape factor f of 1.0 was adopted following Cuffey and Paterson (2010), as both glaciers are wide relative to their thickness. Ice thickness estimates from inversion modelling by Millan and others (2022) were used as a first order estimate, adjusted from their 2021 values to other years using Hugonnet and others (2021) and ArcticDEM glacier elevation change rates. Any surface motion that cannot be attributed to internal deformation is assumed to be due to basal sliding.

Our calculations suggest that basal sliding remains an important contributor to flow across both glaciers from 2000-2024 (Fig. 20), and that its relative contribution is highest in the lower glacier where ice is thinnest. At Illaulittuuq Glacier, motion attributed to basal sliding ranged from 50 to 83% of total surface velocity, with the highest proportions consistently in the 5-10 km zone (75-83%) and lower proportions in the upper glacier (50-64% between 20-35 km). At Maattatujana Glacier, basal sliding accounted for 45-85% of motion, highest near the terminus (79-85% in the 0-5 km zone) and generally decreasing upglacier.

Despite basal sliding remaining important throughout, a general trend toward a larger fraction of total motion due to ice deformation (i.e., less basal sliding) is apparent over time, most clearly in the mid to lower sections of both glaciers. At Illaulittuuq Glacier, the most notable decreases occurred in the 10-15 km and 15-20 km zones, where basal sliding declined by 9.1% and 9.0% of the total velocity, respectively, between 2000-04 and 2020-24, with smaller but consistent decreases across most other sections. At Maattatujana Glacier, a similar pattern emerged in the mid to lower glacier, with the relative importance of basal sliding in the 5-10 km and 10-15 km zones declining by 8.5% and 8.0% of the total velocity, respectively, over the same interval. These reductions in the importance of basal sliding are concentrated where thinning has been greatest, pointing to a common driver. As ice thins, driving stress and overburden pressure decline, meltwater drainage becomes more channelized and efficient, and reduced ice thickness lowers the closure rate of subglacial channels (Perol and others, 2015), all of which act to suppress basal sliding (Harcourt and others, 2020; Armstrong and others, 2022). This is consistent with observations across Penny Ice Cap outlet glaciers by Schaffer and others (2017), who documented a shift from basal-sliding-dominated flow toward motion increasingly governed by internal deformation between 1985 and 2014, and suggested that this transition accelerates as glacier thinning progresses.

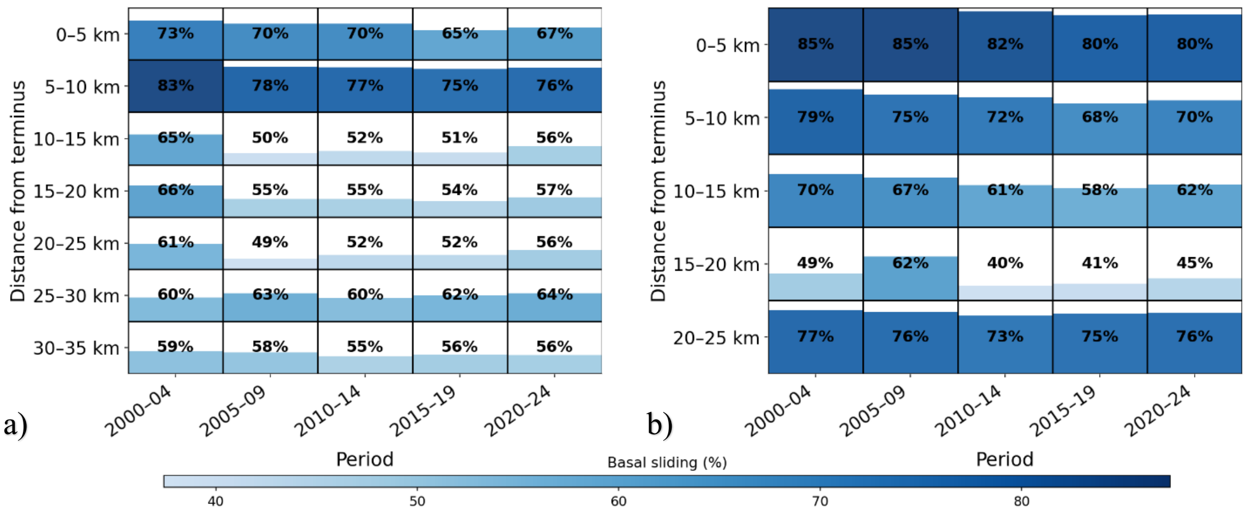

Figure 20. Spatial and temporal variation in the proportion of glacier motion attributed to basal sliding at (a) Illaulittuuq and (b) Maattatujana glaciers from 2000-2024, based on the proportion of motion that cannot be accounted for from internal deformation using Glen's Flow Law.

While the deformation contribution calculations provide insight into the long-term partitioning of glacier flow, they rely on assumptions regarding ice temperature, thickness, and geometry that introduce uncertainty into the absolute values. To provide an independent measure of the importance of basal sliding versus internal deformation in accounting for total glacier motion, seasonal velocity records can also be used. For this, seasonal velocity excess was quantified using annual velocity time series from the ITS_LIVE velocity mosaic (2000-2024). For each location along the glacier centerline, we calculated seasonal median velocities for winter (DJF), spring (MAM), summer (JJA), and autumn (SON), then computed the annual mean velocity as the median of available seasonal values. Seasonal velocity excess was defined as the difference between annual mean velocity and winter velocity, expressed as a percentage of annual motion. Winter velocity was used as the baseline because it represents ice motion with minimal meltwater influence. This excess velocity above the winter baseline is interpreted primarily as meltwater-driven basal motion (Bingham and others, 2008), providing an independent indication of how the importance of basal sliding has evolved through time.

Seasonal velocity excess (i.e., basal sliding) was highest across both glaciers during 2005-2014, before declining substantially after 2015 (Fig. 21). The largest reductions occurred within the mid-glacier sections of both glaciers, whereas the lowermost sections experienced comparatively little change. At Maattatujana, excess values in the 5-10 km and 10-15 km zones peaked at 43-51% during 2005-2014 before declining to 18% and 11%, respectively, by 2020-

2024. At Illaulittuuq Glacier, the decline was more spatially extensive than at Maattatujana. The clearest and most consistent reductions occurred within the central glacier (10-25 km from the terminus), where seasonal velocity excess decreased from approximately 23-33% during 2005-2014 to 10-15% by 2020-2024. These reductions coincide with the regions of the glacier that exhibited the largest reductions in basal sliding outlined in the previous section (Fig. 20).

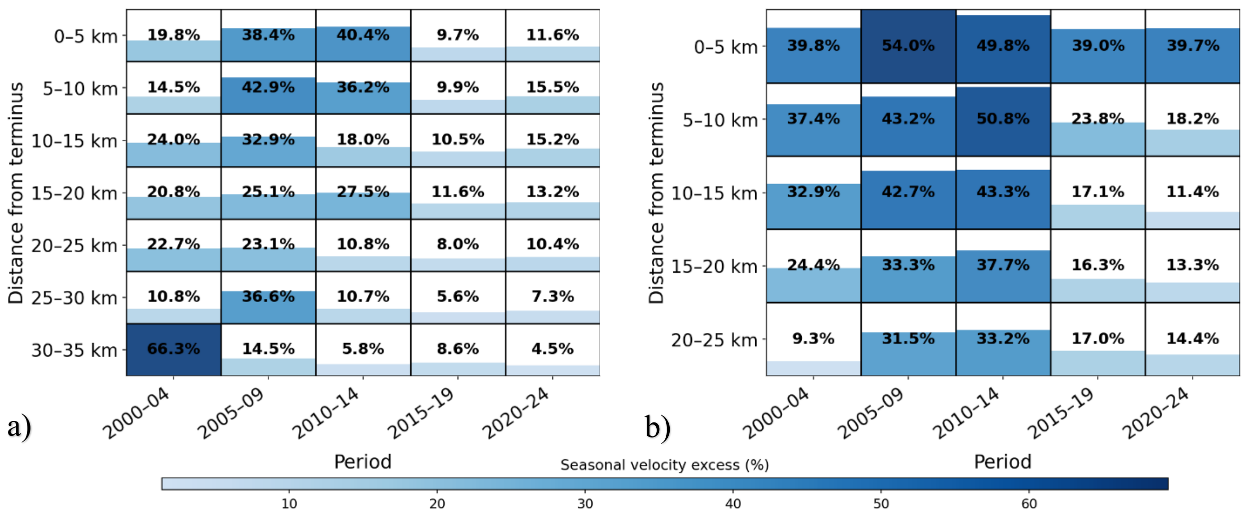

Figure 21. Seasonal velocity excess (assumed to indicate basal sliding rates) at: (a) Illaulittuuq and (b) Maattatujana glaciers from 2000-2024, calculated as the proportion of annual surface velocity occurring above winter (DJF) flow conditions.

Although the seasonal velocity excess remains consistently lower than the basal sliding fractions derived from the deformation calculations (likely because it captures only the seasonally varying component of glacier motion, whereas the deformation analysis accounts for all non-deformation motion throughout the year), both approaches identify the same broad pattern: a decrease in the importance of basal sliding over time. The seasonal velocity excess data allow this decrease to be examined more specifically through its meltwater-sensitive component, which shows a marked decline after 2014. This decline therefore provides independent support for the interpretation that internal deformation constitutes an increasingly larger proportion of total glacier motion, and basal sliding is becoming increasingly less important. This is not because ice deformation is increasing, but because the meltwater-driven component of motion is declining more rapidly, particularly within the thinning mid-glacier regions of both glaciers.

A third line of evidence supporting this interpretation is the pronounced asymmetry in long-term seasonal deceleration rates observed at both glaciers (Fig. 15). Within the zones of greatest statistical significance, the lower 26.5 km at Illaulittuuq and the lower 15 km at Maattatujana, spring and summer deceleration rates are two to four times greater than those observed in winter and fall. This seasonal asymmetry is consistent with the meltwater-sensitive component of glacier motion (i.e., basal sliding) declining more rapidly than the background component of flow (i.e., internal deformation). Because spring and summer velocities are most strongly influenced by seasonal meltwater inputs, they would be expected to respond most strongly to any long-term reduction in meltwater-driven acceleration associated with glacier thinning and increasingly efficient subglacial drainage. Winter velocity, by contrast, is least influenced by seasonal meltwater inputs and therefore provides the closest available proxy for the deformation-dominated component of flow. Its comparatively slow rate of decline suggests that this component of motion has remained more stable through time, responding primarily to gradual changes in ice thickness and surface slope rather than to interannual variations in meltwater supply.

Similar patterns have been documented elsewhere on Penny Ice Cap (Schaffer and others, 2017), and the CAA (Van Wychen and others, 2020a), where thinning-driven reductions in basal sliding were likewise associated with a diminishing influence of seasonal meltwater-driven acceleration on glacier flow. Under continued atmospheric warming and projected future mass losses (Rounce and others, 2023), notably concentrated at low elevations across Penny Ice Cap (Schaffer and others, 2023), this pattern is expected to intensify, with deformation-dominated flow expanding progressively upglacier as thinning propagates beyond the lower glacier.

2.6 Summary and Conclusions

Based on analysis of multidecadal changes at Illaulittuuq and Maattatujana glaciers from 1958-2024, this study demonstrates that both glaciers have undergone sustained retreat, thinning, and deceleration despite their contrasting terminus types. Their remarkably similar long-term behaviour indicates that recent glacier evolution is governed primarily by a shared response to climatic forcing, rather than by differences in terminus setting. Although Illaulittuuq Glacier remains marine-terminating, the progressive decline in dynamic discharge towards present day suggests that frontal processes exert an increasingly limited influence on its overall behaviour. Instead, glacier thinning has emerged as the dominant control on glacier dynamics at both sites, with internal deformation representing an increasingly larger proportion of total glacier motion through time. While this pattern of increasing deformation-dominated flow is consistent with observations from other glacierized regions experiencing sustained negative mass balance, including the CAA (Schaffer and others, 2017; Thomson and Copland, 2017), Alaska and Patagonia (Heid and Kääb, 2012), and the Himalayas (Ghosh and others, 2026), this study advances understanding of the underlying process driving this shift. Rather than reflecting an increase in deformation itself, this shift is primarily driven by a decline in the meltwater-enhanced component of basal sliding, particularly during the spring and summer melt seasons. Through its influence on subglacial hydrology, continued thinning has reduced basal water pressure, decreasing closure rates of subglacial channels and promoting a shift toward more efficient channelized drainage. This leads to increased meltwater evacuation efficiency which, in turn, diminished the relative contribution of basal sliding to total glacier flow.

In contrast, these results differ from observations in parts of the northern CAA (Harcourt and others, 2020) and Greenland (King and others, 2020), where dynamic thinning has been accompanied by increased velocities and enhanced basal sliding. These contrasting responses highlight the strong regional variability in glacier adjustment to climate warming and demonstrate the importance of glacier geometry, terminus conditions, and local dynamic controls in governing glacier evolution. In the southern Canadian Arctic, where glaciers are highly sensitive to atmospheric warming (Rodríguez-Cuicas and others, 2023), and mass loss has accelerated substantially in recent decades (Millan and others, 2017; Noël and others, 2018), the trajectories observed at Illaulittuuq and Maattatujana glaciers suggest that thinning-driven retreat and velocity reductions are becoming increasingly important controls on glacier evolution and flow dynamics. Identifying the mechanism underlying this shift improves understanding of how glaciers with limited marine influence, sustained thinning, and progressive velocity reduction are likely to evolve, providing a more physically grounded basis for representing these dynamics in predictive models and improving projections of future glacier contributions to regional sea-level rise and freshwater discharge.

Looking ahead, Maattatujana Glacier may provide a useful analogue for the near-future evolution of Illaulittuuq Glacier, illustrating how a glacier can continue to lose mass and retreat under predominantly atmospheric forcing with limited influence from frontal processes. If Illaulittuuq continues to evolve toward a more land-terminating style of behaviour, its long-term evolution becomes increasingly predictable, characterized by continued thinning, retreat, deceleration, and reduced ice delivery to the terminus. Such a transition would likely further reduce Illaulittuuq Glacier's already modest contribution from dynamic discharge, with continued thinning promoting velocity reductions that propagate progressively upglacier. As a result, Illaulittuuq Glacier may increasingly resemble Maattatujana Glacier, exhibiting lower velocities throughout the glacier and a flow regime controlled predominantly by thinning and reduced driving stress. Reduced ice delivery to the terminus may also promote the accumulation and persistence of supraglacial debris near the glacier margin as less mass is evacuated through calving. However, without bed topography data, it is not possible to determine whether future retreat will expose an overdeepened basin capable of triggering renewed dynamic activity associated with marine instability. Consequently, while Illaulittuuq presently behaves more similarly to a land-terminating glacier than an actively dynamic marine-terminating glacier, the possibility of future dynamic reactivation cannot be excluded (Haritashya and others, 2015).

Beyond advancing our understanding of glacier dynamics on southern Baffin Island and similar regions, this work provides an important regional baseline for assessing future environmental change across the Penny Ice Cap region. Continued glacier mass loss will influence freshwater delivery, sediment transport, fiord conditions, and iceberg production, with consequences for coastal ecosystems (Bhatia et al., 2021) surrounding Qikiqtarjuaq. These environmental changes are particularly important for Inuit communities that rely on these environments for harvesting, travel, and tourism. By documenting how two of Penny Ice Cap's largest outlet glaciers have responded to more than six decades of climate-driven change, these findings improve our understanding of how Arctic glacier systems are responding to modern warming and reinforce the need to consider regional variability when assessing the future of the Canadian Arctic cryosphere.

Chapter 3: References

Abdalati, W., Krabill, W., Frederick, E., Manizade, S., Martin, C., Sonntag, J., Swift, R., Thomas, R., Yungel, J., & Koerner, R. (2004). Elevation changes of ice caps in the Canadian Arctic Archipelago. *Journal of Geophysical Research: Earth Surface*, *109*(F4), 2003JF000045. https://doi.org/10.1029/2003JF000045

Ali, A., Dunlop, P., Coleman, S., Kerr, D., McNabb, R. W., & Noormets, R. (2023). Glacier area changes in the Arctic and high latitudes using satellite remote sensing. *Journal of Maps*, *19*(1), 1–7. https://doi.org/10.1080/17445647.2023.2247416

Alley, R. B. (2000). Continuity comes first: Recent progress in understanding subglacial deformation. *Deformation of Glacial Materials*, *176*(1), 171–179.

Alley, R. B., Blankenship, D. D., Bentley, C. R., & Rooney, S. T. (1986). Deformation of till beneath ice stream B, West Antarctica. *Nature*, *322*(6074), 57–59. https://doi.org/10.1038/322057a0

Amundson, J. M. (2016). A mass-flux perspective of the tidewater glacier cycle. *Journal of Glaciology*, *62*(231), 82–93. https://doi.org/10.1017/jog.2016.14

Anderson, B., Willis, I., Goodsell, B., Banwell, A., Owens, I., Mackintosh, A., & Lawson, W. (2014). Annual to Daily Ice Velocity and Water Pressure Variations on Ka Roimata o Hine Hukatere (Franz Josef Glacier), New Zealand. *Arctic, Antarctic, and Alpine Research*, *46*(4), 919–932. https://doi.org/10.1657/1938-4246-46.4.919

Armstrong, W. H., Polashenski, D., Truffer, M., Horne, G., Hanson, J. B., Hawley, R. L., Hengst, A. M., Vowels, L., Menounos, B., & Wychen, W. V. (2022). Declining Basal Motion Dominates the Long-Term Slowing of Athabasca Glacier, Canada. *Journal of Geophysical Research: Earth Surface*, *127*(10), e2021JF006439. https://doi.org/10.1029/2021JF006439

Bader, H. (1954). Sorge's law of densification of snow on high polar glaciers. *Journal of Glaciology*, *2*, 319–323.

Berthier, E., Arnaud, Y., Kumar, R., Ahmad, S., Wagnon, P., & Chevallier, P. (2007). Remote sensing estimates of glacier mass balances in the Himachal Pradesh (Western Himalaya, India). *Remote Sensing of Environment*, *108*(3), 327–338. https://doi.org/10.1016/j.rse.2006.11.017

Bhatia, M. P., Waterman, S., Burgess, D. O., Williams, P. L., Bundy, R. M., Mellett, T., Roberts, M., & Bertrand, E. M. (2021). Glaciers and Nutrients in the Canadian Arctic Archipelago Marine System. *Global Biogeochemical Cycles*, *35*(8), e2021GB006976. https://doi.org/10.1029/2021GB006976

Bingham, R. G., Hubbard, A. L., Nienow, P. W., & Sharp, M. J. (2008). An investigation into the mechanisms controlling seasonal speedup events at a High Arctic glacier. *Journal of Geophysical Research: Earth Surface*, *113*(F2), 2007JF000832. https://doi.org/10.1029/2007JF000832

Boulton, G. S., & Hindmarsh, R. C. A. (1987). Sediment deformation beneath glaciers: Rheology and geological consequences. *Journal of Geophysical Research: Solid Earth*, *92*(B9), 9059–9082. https://doi.org/10.1029/JB092iB09p09059

Box, J. E., Colgan, W. T., Wouters, B., Burgess, D. O., O'Neel, S., Thomson, L. I., & Mernild, S. H. (2018). Global sea-level contribution from Arctic land ice: 1971–2017. *Environmental Research Letters*, *13*(12), 125012. https://doi.org/10.1088/1748-9326/aaf2ed

Box, J. E., & Sharp, M. (2017). Changes to Arctic land ice. In *Snow, Water, Ice and Permafrost in the Arctic (SWIPA) 2017* (pp. 137–168). Arctic Monitoring and Assessment Programme (AMAP).

Braithwaite, R. J., & Hughes, P. D. (2020). Regional Geography of Glacier Mass Balance Variability Over Seven Decades 1946–2015. *Frontiers in Earth Science*, *8*, 302. https://doi.org/10.3389/feart.2020.00302

Brinkerhoff, D., Truffer, M., & Aschwanden, A. (2017). Sediment transport drives tidewater glacier periodicity. *Nature Communications*, *8*(1), 90. https://doi.org/10.1038/s41467-017-00095-5

Burgess, D. O., Sharp, M. J., Mair, D. W. F., Dowdeswell, J. A., & Benham, T. J. (2005). Flow dynamics and iceberg calving rates of Devon Ice Cap, Nunavut, Canada. *Journal of Glaciology*, *51*(173), 219–230. https://doi.org/10.3189/172756505781829430

Ciracì, E., Velicogna, I., & Swenson, S. (2020). Continuity of the Mass Loss of the World's Glaciers and Ice Caps From the GRACE and GRACE Follow-On Missions. *Geophysical Research Letters*, *47*(9), e2019GL086926. https://doi.org/10.1029/2019GL086926

Cogley, J. (2009). Geodetic and direct mass-balance measurements: Comparison and joint analysis. *Annals of Glaciology*, *50*(50), 96–100. https://doi.org/10.3189/172756409787769744

Cogley, J. G., Hock, R., Rasmussen, L. A., Arendt, A. A., Bauder, A., Braithwaite, R. J., Kaser, G., Möller, M., Nicholson, L., & Zemp, M. (2011). *Glossary of glacier mass balance and related terms*. International Association of Cryospheric Sciences. https://unesdoc.unesco.org/ark:/48223/pf0000192525

Cook, A. J., Copland, L., Noël, B. P. Y., Stokes, C. R., Bentley, M. J., Sharp, M. J., Bingham, R. G., & Van Den Broeke, M. R. (2019). Atmospheric forcing of rapid marine-terminating glacier retreat in the Canadian Arctic Archipelago. *Science Advances*, *5*(3), eaau8507. https://doi.org/10.1126/sciadv.aau8507

Cuffey, K. M., & Paterson, W. S. B. (2010). *The physics of glaciers* (Fourth edition). Elsevier.

Curley, A. N., Kochtitzky, W. H., Edwards, B. R., & Copland, L. (2021). Glacier changes over the past 144 years at Alexandra Fiord, Ellesmere Island, Canada. *Journal of Glaciology*, *67*(263), 511–522. https://doi.org/10.1017/jog.2021.4

Dai, C., & Howat, I. M. (2017). Measuring Lava Flows With ArcticDEM: Application to the 2012–2013 Eruption of Tolbachik, Kamchatka. *Geophysical Research Letters*, *44*(24). https://doi.org/10.1002/2017GL075920

Dalton, A., Van Wychen, W., Copland, L., Gray, L., & Burgess, D. (2022). Seasonal and Multiyear Flow Variability on the Prince of Wales Icefield, Ellesmere Island: 2009–2019. *Journal of Geophysical Research: Earth Surface*, *127*(4), e2021JF006501. https://doi.org/10.1029/2021JF006501

Dehecq, A., Gourmelen, N., Gardner, A. S., Brun, F., Goldberg, D., Nienow, P. W., Berthier, E., Vincent, C., Wagnon, P., & Trouvé, E. (2019). Twenty-first century glacier slowdown driven by mass loss in High Mountain Asia. *Nature Geoscience*, *12*(1), 22–27. https://doi.org/10.1038/s41561-018-0271-9

Fisher, D., Zheng, J., Burgess, D., Zdanowicz, C., Kinnard, C., Sharp, M., & Bourgeois, J. (2011). Recent melt rates of Canadian arctic ice caps are the highest in four millennia. *Global and Planetary Change*, *84–85*, 3–7. https://doi.org/10.1016/j.gloplacha.2011.06.005

Gardelle, J., Berthier, E., & Arnaud, Y. (2012). Slight mass gain of Karakoram glaciers in the early twenty-first century. *Nature Geoscience*, *5*(5), 322–325. https://doi.org/10.1038/ngeo1450

Gardner, A., Moholdt, G., Arendt, A., & Wouters, B. (2012). Accelerated contributions of Canada's Baffin and Bylot Island glaciers to sea level rise over the past half century. *The Cryosphere*, *6*(5), 1103–1125. https://doi.org/10.5194/tc-6-1103-2012

Gardner, A. S., Greene, C. A., Kennedy, J. H., Fahnestock, M. A., Liukis, M., López, L. A., Lei, Y., Scambos, T. A., & Dehecq, A. (2025). *ITS_LIVE global glacier velocity data in near real time*. https://doi.org/10.5194/egusphere-2025-392

Gardner, A. S., Moholdt, G., Cogley, J. G., Wouters, B., Arendt, A. A., Wahr, J., Berthier, E., Hock, R., Pfeffer, W. T., Kaser, G., Ligtenberg, S. R. M., Bolch, T., Sharp, M. J., Hagen, J. O., Van Den Broeke, M. R., & Paul, F. (2013). A Reconciled Estimate of Glacier Contributions to Sea Level Rise: 2003 to 2009. *Science*, *340*(6134), 852–857. https://doi.org/10.1126/science.1234532

Gardner, A. S., Moholdt, G., Wouters, B., Wolken, G. J., Burgess, D. O., Sharp, M. J., Cogley, J. G., Braun, C., & Labine, C. (2011). Sharply increased mass loss from glaciers and ice caps in the Canadian Arctic Archipelago. *Nature*, *473*(7347), 357–360. https://doi.org/10.1038/nature10089

Ghosh, T., Ramsankaran, R., McCormack, F. S., & Mackintosh, A. N. (2026). Thinning-induced glacier deceleration in the Zanskar Himalayas. *The Cryosphere*, *20*(6), 3415–3433. https://doi.org/10.5194/tc-20-3415-2026

Glen, J. W. (1958). In *The flow law of ice: A discussion of the assumptions made in glacier theory, their experimental foundations and consequences* (Vol. 47, pp. 171–183). IASH Publ.

Greene, C. A., & Gardner, A. S. (2025). Seasonal dynamics of Earth's glaciers and ice sheets. *Science*, *390*(6776), 945–950. https://doi.org/10.1126/science.adx6654

Hall, D. K., Bayr, K. J., Schöner, W., Bindschadler, R. A., & Chien, J. Y. L. (2003). Consideration of the errors inherent in mapping historical glacier positions in Austria from the ground and space (1893–2001). *Remote Sensing of Environment*, *86*(4), 566–577. https://doi.org/10.1016/S0034-4257(03)00134-2

Harcourt, W. D., Palmer, S. J., Mansell, D. T., Le Brocq, A., Bartlett, O., Gourmelen, N., Tepes, P., Dowdeswell, J. A., Blankenship, D. D., & Young, D. A. (2020). Subglacial controls on dynamic thinning at Trinity-Wykeham Glacier, Prince of Wales Ice Field, Canadian

Arctic. *International Journal of Remote Sensing*, *41*(3), 1191–1213. https://doi.org/10.1080/01431161.2019.1658238

Harig, C., & Simons, F. J. (2016). Ice mass loss in Greenland, the Gulf of Alaska, and the Canadian Archipelago: Seasonal cycles and decadal trends. *Geophysical Research Letters*, *43*(7), 3150–3159. https://doi.org/10.1002/2016GL067759

Heid, T., & Kääb, A. (2012). Repeat optical satellite images reveal widespread and long term decrease in land-terminating glacier speeds. *The Cryosphere*, *6*(2), 467–478. https://doi.org/10.5194/tc-6-467-2012

Hersbach, H., Bell, B., Berrisford, P., Biavati, G., Horányi, A., Muñoz Sabater, J., Nicolas, J., Peubey, C., Radu, R., Rozum, I., Schepers, D., Simmons, A., Soci, C., Dee, D., & Thépaut, J.-N. (2019). *ERA5 monthly averaged data on single levels from 1940 to present* [Dataset]. opernicus Climate Change Service (C3S) Climate Data Store (CDS). https://doi.org/10.24381/cds.f17050d7

Huang, L., & Li, Z. (2011). Comparison of SAR and optical data in deriving glacier velocity with feature tracking. *International Journal of Remote Sensing*, *32*(10), 2681–2698. https://doi.org/10.1080/01431161003720395

Hubbard, B., & Sharp, M. (1995). Basal Ice Fades and Their Formation in the Western Alps. *Arctic and Alpine Research*, *27*(4), 301–310. https://doi.org/10.1080/00040851.1995.12003127

Hugonnet, R., McNabb, R., Berthier, E., Menounos, B., Nuth, C., Girod, L., Farinotti, D., Huss, M., Dussaillant, I., Brun, F., & Kääb, A. (2021). Accelerated global glacier mass loss in the early twenty-first century. *Nature*, *592*(7856), 726–731. https://doi.org/10.1038/s41586-021-03436-z

Huss, M. (2013). Density assumptions for converting geodetic glacier volume change to mass change. *The Cryosphere*, *7*(3), 877–887. https://doi.org/10.5194/tc-7-877-2013

Iken, A. (1981). The Effect of the Subglacial Water Pressure on the Sliding Velocity of a Glacier in an Idealized Numerical Model. *Journal of Glaciology*, *27*(97), 407–421. https://doi.org/10.3189/S0022143000011448

IPCC. (2019). *IPCC Special Report on the Ocean and Cryosphere in a Changing Climate* (p. 755). Cambridge University Press. https://doi.org/10.1017/9781009157964

IPCC. (2023a). *Climate Change 2021 – The Physical Science Basis* (p. 2214). Cambridge University Press. https://doi.org/10.1017/9781009157896

IPCC. (2023b). *Climate Change 2023: Synthesis Report. Contribution of Working Groups I, II and III to the Sixth Assessment Report of the Intergovernmental Panel on Climate Change* (First). Intergovernmental Panel on Climate Change (IPCC). https://doi.org/10.59327/IPCC/AR6-9789291691647

Jacob, T., Wahr, J., Pfeffer, W. T., & Swenson, S. (2012). Recent contributions of glaciers and ice caps to sea level rise. *Nature*, *482*(7386), 514–518. https://doi.org/10.1038/nature10847

Jansen, E., Christensen, J. H., Dokken, T., Nisancioglu, K. H., Vinther, B. M., Capron, E., Guo, C., Jensen, M. F., Langen, P. L., Pedersen, R. A., Yang, S., Bentsen, M., Kjær, H. A., Sadatzki, H., Sessford, E., & Stendel, M. (2020). Past perspectives on the present era of abrupt Arctic climate change. *Nature Climate Change*, *10*(8), 714–721. https://doi.org/10.1038/s41558-020-0860-7

Jiskoot, H. (2011). Dynamics of glaciers. In *Encyclopedia of snow, ice and glaciers* (pp. 245–256). Springer, Dordrecht. https://agupubs.onlinelibrary.wiley.com/doi/10.1029/2003JF000082

Kamb, B. (1987). Glacier surge mechanism based on linked cavity configuration of the basal water conduit system. *Journal of Geophysical Research: Solid Earth*, *92*(B9), 9083–9100. https://doi.org/10.1029/JB092iB09p09083

Kochtitzky, W., & Copland, L. (2022). Retreat of Northern Hemisphere Marine-Terminating Glaciers, 2000–2020. *Geophysical Research Letters*, *49*. https://doi.org/10.1029/2021GL096501

Larsen, C. F., Burgess, E., Arendt, A. A., O'Neel, S., Johnson, A. J., & Kienholz, C. (2015). Surface melt dominates Alaska glacier mass balance. *Geophysical Research Letters*, *42*(14), 5902–5908. https://doi.org/10.1002/2015GL064349

Lauzon, B., Copland, L., Van Wychen, W., Kochtitzky, W., McNabb, R., & Dahl-Jensen, D. (2023). Dynamics throughout a complete surge of Iceberg Glacier on western Axel Heiberg Island, Canadian High Arctic. *Journal of Glaciology*, *69*(277), 1333–1350. https://doi.org/10.1017/jog.2023.20

Lliboutry, L. (1968). General Theory of Subglacial Cavitation and Sliding of Temperate Glaciers. *Journal of Glaciology*, *7*(49), 21–58. https://doi.org/10.3189/S0022143000020396

Main, B., Copland, L., Smeda, B., Kochtitzky, W., Samsonov, S., Dudley, J., Skidmore, M., Dow, C., Van Wychen, W., Medrzycka, D., Higgs, E., & Mingo, L. (2023). Terminus change of Kaskawulsh Glacier, Yukon, under a warming climate: Retreat, thinning, slowdown and modified proglacial lake geometry. *Journal of Glaciology*, *69*(276), 936–952. https://doi.org/10.1017/jog.2022.114

Małecki, J. (2022). Recent contrasting behaviour of mountain glaciers across the European High Arctic revealed by ArcticDEM data. *The Cryosphere*, *16*(5), 2067–2082. https://doi.org/10.5194/tc-16-2067-2022

Marzeion, B., Jarosch, A. H., & Hofer, M. (2012). Past and future sea-level change from the surface mass balance of glaciers. *The Cryosphere*, *6*(6), 1295–1322. https://doi.org/10.5194/tc-6-1295-2012

Medrzycka, D., Copland, L., & Noël, B. (2023). Rapid demise and committed loss of Bowman Glacier, northern Ellesmere Island, Arctic Canada. *Journal of Glaciology*, *69*(276), 997–1010. https://doi.org/10.1017/jog.2022.119

Millan, R., Mouginot, J., Rabatel, A., & Morlighem, M. (2022). Ice velocity and thickness of the world's glaciers. *Nature Geoscience*, *15*(2), 124–129. https://doi.org/10.1038/s41561-021-00885-z

Millan, R., Mouginot, J., & Rignot, E. (2017). Mass budget of the glaciers and ice caps of the Queen Elizabeth Islands, Canada, from 1991 to 2015. *Environmental Research Letters*, *12*(2), 024016. https://doi.org/10.1088/1748-9326/aa5b04

Moholdt, G., Nuth, C., Hagen, J. O., & Kohler, J. (2010). Recent elevation changes of Svalbard glaciers derived from ICESat laser altimetry. *Remote Sensing of Environment*, *114*(11), 2756–2767. https://doi.org/10.1016/j.rse.2010.06.008

Mortimer, C. A., Sharp, M., & Wouters, B. (2016). Glacier surface temperatures in the Canadian High Arctic, 2000–15. *Journal of Glaciology*, *62*(235), 963–975. https://doi.org/10.1017/jog.2016.80

NOAA National Centers for Environmental information. (2024). *Climate at a Glance: Global Time Series* [Dataset]. https://www.ncei.noaa.gov/access/monitoring/climate-at-a-glance/global/time-series

Noël, B., Van De Berg, W. J., Lhermitte, S., Wouters, B., Schaffer, N., & Van Den Broeke, M. R. (2018). Six Decades of Glacial Mass Loss in the Canadian Arctic Archipelago. *Journal of Geophysical Research: Earth Surface*, *123*(6), 1430–1449. https://doi.org/10.1029/2017JF004304

Noh, M.-J., & Howat, I. M. (2015). Automated stereo-photogrammetric DEM generation at high latitudes: Surface Extraction with TIN-based Search-space Minimization (SETSM) validation and demonstration over glaciated regions. *GIScience & Remote Sensing*, *52*(2), 198–217. https://doi.org/10.1080/15481603.2015.1008621

Partington, G., Copland, L., Lauzon, B., Medrzycka, D., Main, B., Kochtitzky, W. H., & Dow, C. F. (2025). Surge history and dynamics of Fisher Glacier, Yukon, 1948–2022. *Journal of Glaciology*, *71*, e100. https://doi.org/10.1017/jog.2025.10084

Paterson, W. S. B. (1994). *The Physics of Glaciers* (3rd ed.). Pergamon.

Perol, T., Rice, J. R., Platt, J. D., & Suckale, J. (2015). Subglacial hydrology and ice stream margin locations. *Journal of Geophysical Research: Earth Surface*, *120*(7), 1352–1368. https://doi.org/10.1002/2015JF003542

Pimentel, S., Flowers, G. E., Sharp, M. J., Danielson, B., Copland, L., Van Wychen, W., Duncan, A., & Kavanaugh, J. L. (2017). Modelling intra-annual dynamics of a major marine-terminating Arctic glacier. *Annals of Glaciology*, *58*(74), 118–130. https://doi.org/10.1017/aog.2017.23

Porter, C., Howat, I., Noh, M.-J., Husby, E., Khuvis, S., Danish, E., Tomko, K., Gardiner, J., Negrete, A., Yadav, B., Klassen, J., Kelleher, C., Cloutier, M., Bakker, J., Enos, J., Arnold, G., Bauer, G., Morin, P., & Polar Geospatial Center. (2022). *ArcticDEM - Strips, Version 4.1* (Version 1.4) [Dataset]. Harvard Dataverse. https://doi.org/10.7910/DVN/C98DVS

Rantanen, M., Karpechko, A. Yu., Lipponen, A., Nordling, K., Hyvärinen, O., Ruosteenoja, K., Vihma, T., & Laaksonen, A. (2022). The Arctic has warmed nearly four times faster than the globe since 1979. *Communications Earth & Environment*, *3*(1), 168. https://doi.org/10.1038/s43247-022-00498-3

RGI 7.0 Consortium. (2023). *Randolph Glacier Inventory – A dataset of global glacier outlines, version 7.0* [Dataset]. National Snow and Ice Data Center (NSIDC). https://doi.org/10.5067/F6JMOVY5NAVZ

Rodríguez-Cuicas, M.-E., Montero-Serrano, J.-C., St-Onge, G., & Normandeau, A. (2023). A 600-year marine record associated with the dynamics of the eastern Penny Ice Cap (Baffin Island, Nunavut, Canada). *Journal of Quaternary Science*, *38*(7), 1062–1081. https://doi.org/doi.org/10.1002/jqs.3531

Rounce, D. R., Hock, R., Maussion, F., Hugonnet, R., Kochtitzky, W., Huss, M., Berthier, E., Brinkerhoff, D., Compagno, L., Copland, L., Farinotti, D., Menounos, B., & McNabb, R. W. (2023). Global glacier change in the 21st century: Every increase in temperature matters. *Science*, *379*(6627), 78–83. https://doi.org/10.1126/science.abo1324

Sapiano, J. J., Harrison, W. D., & Echelmeyer, K. A. (1998). Elevation, volume and terminus changes of nine glaciers in North America. *Journal of Glaciology*, *44*(146), 119–135. https://doi.org/10.3189/S0022143000002410

Schaffer, N., Copland, L., & Zdanowicz, C. (2017). Ice velocity changes on Penny Ice Cap, Baffin Island, since the 1950s. *Journal of Glaciology*, *63*(240), 716–730. https://doi.org/10.1017/jog.2017.40

Schaffer, N., Copland, L., Zdanowicz, C., Burgess, D., & Nilsson, J. (2020). Revised Estimates of Recent Mass Loss Rates for Penny Ice Cap, Baffin Island, Based on 2005–2014 Elevation Changes Modified for Firn Densification. *Journal of Geophysical Research: Earth Surface*, *125*(8), e2019JF005440. https://doi.org/10.1029/2019JF005440

Schaffer, N., Copland, L., Zdanowicz, C., & Hock, R. (2023). Modeling the surface mass balance of Penny Ice Cap, Baffin Island, 1959–2099. *Annals of Glaciology*, 1–13. https://doi.org/10.1017/aog.2023.68

Sharp, M., Ananicheva, M., Arendt, A., Hagen, J. O., Hock, R., Josberger, E., Moore, R. D., Pfeffer, W. T., & Wolken, G. J. (2011). Mountain glaciers and ice caps. In *Snow, water, ice and permafrost in the Arctic (SWIPA): Climate change and the cryosphere* (pp. 1–61). Arctic Monitoring and Assessment Program.

Sharp, M., Wolken, G., Burgess, D., Cogley, J. G., Copland, L., Thomson, L., Arendt, A., Wouters, B., Kohler, J., Andreassen, L. M., O'Neel, S., & Pelto, M. (2015). Glaciers and ice caps outside Greenland. In *State of the Climate in 2014* (Vol. 96, pp. S135–S137). Bulletin of the American Meteorological Society.

Shepherd, A., Ivins, E. R., A, G., Barletta, V. R., Bentley, M. J., Bettadpur, S., Briggs, K. H., Bromwich, D. H., Forsberg, R., Galin, N., Horwath, M., Jacobs, S., Joughin, I., King, M. A., Lenaerts, J. T. M., Li, J., Ligtenberg, S. R. M., Luckman, A., Luthcke, S. B., … Zwally, H. J. (2012). A Reconciled Estimate of Ice-Sheet Mass Balance. *Science*, *338*(6111), 1183–1189. https://doi.org/10.1126/science.1228102

Shi, L., Allen, C. T., Ledford, J. R., Rodriguez-Morales, F., Blake, W. A., Panzer, B. G., Prokopiack, S. C., Leuschen, C. J., & Gogineni, S. (2010). Multichannel Coherent Radar Depth Sounder for NASA Operation Ice Bridge. *2010 IEEE International Geoscience and Remote Sensing Symposium*, 1729–1732. https://doi.org/10.1109/IGARSS.2010.5649518

Statistics Canada. (2017). *Qikiqtarjuaq, HAM [Census subdivision], Nunavut and Grise Fiord, HAM [Census subdivision], Nunavut (table)* (Nos. 98-316-X2016001; Census Profile). https://www12.statcan.gc.ca/census-recensement/2016/dp-pd/prof/index.cfm?Lang=E

Syvitski, J., Andrews, J. T., Schafer, C. T., & Stravers, J. A. (2022). Sediment fill of Baffin Island fjords: Architecture and rates. *Quaternary Science Reviews*, *284*, 107474. https://doi.org/10.1016/j.quascirev.2022.107474

Thomson, L., & Copland, L. (2016). White Glacier 2014, Axel Heiberg Island, Nunavut: Mapped using Structure from Motion methods. *Journal of Maps*, *12*(5), 1063–1071. https://doi.org/10.1080/17445647.2015.1124057

Thomson, L. I., & Copland, L. (2017a). Changing contribution of peak velocity events to annual velocities following a multi-decadal slowdown at White Glacier. *Annals of Glaciology*, *58*(75pt2), 145–154. https://doi.org/10.1017/aog.2017.46

Thomson, L. I., & Copland, L. (2017b). Multi-decadal reduction in glacier velocities and mechanisms driving deceleration at polythermal White Glacier, Arctic Canada. *Journal of Glaciology*, *63*(239), 450–463. https://doi.org/10.1017/jog.2017.3

Thomson, L. I., Zemp, M., Copland, L., Cogley, J. G., & Ecclestone, M. A. (2017). Comparison of geodetic and glaciological mass budgets for White Glacier, Axel Heiberg Island, Canada. *Journal of Glaciology*, *63*(237), 55–66. https://doi.org/10.1017/jog.2016.112

Truffer, M., Harrison, W. D., & Echelmeyer, K. A. (2000). Glacier motion dominated by processes deep in underlying till. *Journal of Glaciology*, *46*(153), 213–221. https://doi.org/10.3189/172756500781832909

Truffer, M., & Motyka, R. J. (2016). Where glaciers meet water: Subaqueous melt and its relevance to glaciers in various settings. *Reviews of Geophysics*, *54*(1), 220–239. https://doi.org/10.1002/2015RG000494

Van Wychen, W., Burgess, D., Kochtitzky, W., Nikolic, N., Copland, L., & Gray, L. (2020). RADARSAT-2 Derived Glacier Velocities and Dynamic Discharge Estimates for the Canadian High Arctic: 2015–2020. *Canadian Journal of Remote Sensing*, *46*(6), 695–714. https://doi.org/10.1080/07038992.2020.1859359

Van Wychen, W., Burgess, D. O., Gray, L., Copland, L., Sharp, M., Dowdeswell, J. A., & Benham, T. J. (2014). Glacier velocities and dynamic ice discharge from the Queen Elizabeth Islands, Nunavut, Canada. *Geophysical Research Letters*, *41*(2), 484–490. https://doi.org/10.1002/2013GL058558

Van Wychen, W., Copland, L., & Burgess, D. (2020). Ice Masses of the Eastern Canadian Arctic Archipelago. In O. Slaymaker & N. Catto (Eds.), *Landscapes and Landforms of Eastern Canada* (pp. 297–314). Springer International Publishing. https://doi.org/10.1007/978-3-030-35137-3_13

Van Wychen, W., Copland, L., Burgess, D. O., Gray, L., & Schaffer, N. (2015). Glacier velocities and dynamic discharge from the ice masses of Baffin Island and Bylot Island, Nunavut, Canada. *Canadian Journal of Earth Sciences*, *52*(11), 980–989. https://doi.org/10.1139/cjes-2015-0087

Van Wychen, W., Copland, L., Gray, L., Burgess, D., Danielson, B., & Sharp, M. (2012). Spatial and temporal variation of ice motion and ice flux from Devon Ice Cap, Nunavut, Canada. *Journal of Glaciology*, *58*(210), 657–664. https://doi.org/10.3189/2012JoG11J164

Van Wychen, W., Davis, J., Burgess, D. O., Copland, L., Gray, L., Sharp, M., & Mortimer, C. (2016). Characterizing interannual variability of glacier dynamics and dynamic discharge (1999–2015) for the ice masses of Ellesmere and Axel Heiberg Islands, Nunavut, Canada. *Journal of Geophysical Research: Earth Surface*, *121*(1), 39–63. https://doi.org/10.1002/2015JF003708

Van Wychen, W., Davis, J., Copland, L., Burgess, D. O., Gray, L., Sharp, M., Dowdeswell, J. A., & Benham, T. J. (2017). Variability in ice motion and dynamic discharge from Devon Ice Cap, Nunavut, Canada. *Journal of Glaciology*, *63*(239), 436–449. https://doi.org/10.1017/jog.2017.2

Walsh, J. E. (2014). Intensified warming of the Arctic: Causes and impacts on middle latitudes. *Global and Planetary Change*, *117*, 52–63. https://doi.org/10.1016/j.gloplacha.2014.03.003

Weertman, J. (1957). On the sliding of glaciers. *Journal of Glaciology*, *3*(21), 33–38.

Willis, I. C. (1995). Intra-annual variations in glacier motion: A review. *Progress in Physical Geography: Earth and Environment*, *19*(1), 61–106. https://doi.org/10.1177/030913339501900104

World Glacier Monitoring Service. (2023). *FLUCTUATIONS OF GLACIERS DATABASE (p. 35 MB)* [Dataset]. https://doi.org/https://doi.org/10.5904/WGMS-FOG-2023-09

World Meteorological Organization. (2025). *State of the Global Climate 2025* (2025th ed.). World Meteorological Organization. https://doi.org/10.59327/WMO/S/CRI/SOC/1

Wouters, B., Gardner, A. S., & Moholdt, G. (2019). Global Glacier Mass Loss During the GRACE Satellite Mission (2002-2016). *Frontiers in Earth Science*, *7*, 96. https://doi.org/10.3389/feart.2019.00096

Yu, L., Zhong, S., Vihma, T., & Sun, B. (2021). Attribution of late summer early autumn Arctic sea ice decline in recent decades. *Npj Climate and Atmospheric Science*, *4*(1), 3. https://doi.org/10.1038/s41612-020-00157-4

Zdanowicz, C. M., Fisher, D. A., Clark, I., & Lacelle, D. (2002). An ice-marginal delta O-18 record from Barnes Ice Cap, Baffin Island, Canada. *Annals of Glaciology*, *35*, 145–149. https://doi.org/10.3189/172756402781817031

Zdanowicz, C., Smetny-Sowa, A., Fisher, D., Schaffer, N., Copland, L., Eley, J., & Dupont, F. (2012). Summer melt rates on Penny Ice Cap, Baffin Island: Past and recent trends and implications for regional climate. *Journal of Geophysical Research: Earth Surface*, *117*(F2), 2011JF002248. https://doi.org/10.1029/2011JF002248

Zemp, M., Frey, H., Gärtner-Roer, I., Nussbaumer, S. U., Hoelzle, M., Paul, F., Haeberli, W., Denzinger, F., Ahlstrøm, A. P., Anderson, B., Bajracharya, S., Baroni, C., Braun, L. N., Cáceres, B. E., Casassa, G., Cobos, G., Dávila, L. R., Delgado Granados, H., Demuth, M. N., … Vincent, C. (2015). Historically unprecedented global glacier decline in the early 21st century. *Journal of Glaciology*, *61*(228), 745–762. https://doi.org/10.3189/2015JoG15J017

Zemp, M., Huss, M., Thibert, E., Eckert, N., McNabb, R., Huber, J., Barandun, M., Machguth, H., Nussbaumer, S. U., Gärtner-Roer, I., Thomson, L., Paul, F., Maussion, F., Kutuzov, S.,

& Cogley, J. G. (2019). Global glacier mass changes and their contributions to sea-level rise from 1961 to 2016. *Nature*, *568*(7752), 382–386. https://doi.org/10.1038/s41586-019-1071-0

Zemp, M., Thibert, E., Huss, M., Stumm, D., Rolstad Denby, C., Nuth, C., Nussbaumer, S. U., Moholdt, G., Mercer, A., Mayer, C., Joerg, P. C., Jansson, P., Hynek, B., Fischer, A., Escher-Vetter, H., Elvehøy, H., & Andreassen, L. M. (2013a). Reanalysing glacier mass balance measurement series. *The Cryosphere*, *7*(4), 1227–1245. https://doi.org/10.5194/tc-7-1227-2013

Zemp, M., Thibert, E., Huss, M., Stumm, D., Rolstad Denby, C., Nuth, C., Nussbaumer, S. U., Moholdt, G., Mercer, A., Mayer, C., Joerg, P. C., Jansson, P., Hynek, B., Fischer, A., Escher-Vetter, H., Elvehøy, H., & Andreassen, L. M. (2013b). *Uncertainties and re-analysis of glacier mass balance measurements*. https://doi.org/10.5194/tcd-7-789-2013

Zhou, Y., Chen, J., & Cheng, X. (2021). Glacier Velocity Changes in the Himalayas in Relation to Ice Mass Balance. *Remote Sensing*, *13*(19), 3825. https://doi.org/10.3390/rs13193825

Zoet, L. K., & Iverson, N. R. (2020). A slip law for glaciers on deformable beds. *Science*, *368*(6486), 76–78. https://doi.org/10.1126/science.aaz1183

Zuo, H., Balmaseda, M. A., Tietsche, S., Mogensen, K., & Mayer, M. (2019). The ECMWF operational ensemble reanalysis–analysis system for ocean and sea ice: A description of the system and assessment. *Ocean Science*, *15*(3), 779–808. https://doi.org/10.5194/os-15-779-2019